

Twentieth century Sahel rainfall variability as simulated by the ARPEGE AGCM, and future changes

C. Caminade · L. Terray

Received: 18 August 2008 / Accepted: 18 February 2009 / Published online: 19 March 2009
© Springer-Verlag 2009

Abstract The ability of the ARPEGE AGCM in reproducing the twentieth century Sahelian drought when only forced by observed SST time evolution has been characterized. Atmospheric internal variability is shown to have a strong contribution in driving the simulated precipitation variability over the Sahel at decadal to multi-decadal time scales. The simulated drought is associated with a southward shift of the continental rainbelt over central and eastern Sahel, associated with an inter-hemispheric SST mode (the southern hemisphere oceans warming faster than the northern ones after 1970). The analysis of idealized experiments further highlights the importance of the Pacific basin. The related increase of the tropospheric temperature (TT) over the tropics is then suggested to dry the margin of convection zones over Africa, in agreement with the so-called “upped-ante” mechanism. A simple metric is then defined to determine the ability of the CMIP3 coupled models in reproducing both the observed Sahel drying and these mechanisms, in order to determine the reliability of the twenty-first century scenarios. Only one model reproduces both the observed drought over the Sahel and consistent SST/TT relationships over the second half of the twentieth century. This model predicts enhanced dry conditions over

the Sahel at the end of the twenty-first century. However, as the mechanisms highlighted here for the recent period are not stationary during the twenty-first century when considering the trends, similarities between observed and simulated features of the West African monsoon for the twentieth century are a necessary but insufficient condition for a trustworthy prediction of the future.

Keywords West African monsoon · SST and anthropogenic forcing · Climate scenarios · Decadal to multi-decadal variability · Teleconnection

1 Introduction

The Sahel is the semi-arid transition zone located between the Sahara desert and humid tropical Africa. This region is characterized by strong meridional rainfall gradient and high rainfall variability, with annual rainfall amounts varying from 600 to 700 mm near the Guinean coast to 100–200 mm in the northern part. The vast majority of the Sahel rainfall is associated with the West African monsoon, occurring from July to September, as a result of the northward migration of the Inter Tropical Convergence Zone (ITCZ). Rainfall variability over the Sahel has been characterized by a pronounced multi-decadal trend contrasting a wet (1950s–1970s) and a dry (1970s–1990s) period, followed by a partial recovery over the last decade of the twentieth century. The agrarian activities of the increasing African population strongly depend on the rainy season return, and the persistent drought observed over the 1970–1990 period had dramatic social and economic consequences.

Since the 1980s, the scientific communities efforts to explain this severe drought have taken two main directions. The first point of view, pioneered by Charney et al. (1977),

This paper is a contribution to the special issue on West African Climate, consisting of papers from the African Multidisciplinary Monsoon Analysis (AMMA) and West African Monsoon Modeling and Evaluation (WAMME) projects, and coordinated by Y. Xue and P. M. Ruti.

C. Caminade (✉) · L. Terray
CERFACS, 42 Avenue G. Coriolis,
31057 Toulouse-Cedex, France
e-mail: caminade@cerfacs.fr; cyril.caminade00@gmail.com

L. Terray
e-mail: terray@cerfacs.fr

highlighted regional feedbacks between land surface conditions (soil humidity, vegetation and albedo), atmospheric radiation equilibrium and thus precipitation. In contrast, various studies [following the precursory works of Lamb (1978), Folland et al. (1986), and Palmer (1986)] highlighted the major impact of global sea surface temperature (SST) conditions upon the twentieth century rainfall variability over the Sahel. The recent success of global circulation atmospheric models (GCM) in reproducing the spatio-temporal variability of observed Sahel rainfall when only forced by observed SST time evolution confirmed this mechanism (Giannini et al. 2003, among others) and led to a reactivation of the interest in potential applications such as seasonal forecasting and forecasting of impacts.

At interannual time scales, several studies have highlighted the teleconnection between El Niño Southern oscillation and rainfall variability over the Sahel (Rowell 2001, among others), and the significance of this link during the observed drought (Janicot et al. 2001). Many studies have pointed out the relationship between an interhemispheric SST gradient at global scale (the southern/northern oceans warmed/cooled after 1970) and the Sahelian drought at multi-decadal timescale. More specifically, studies based on simulations have linked the warming of the Indian basin (Bader and Latif 2003, among others), or an increase in the cross-equatorial SST gradient in the Atlantic (Hastenrath 1990) with the ITCZ location. Alternatively, the works of Heger et al. (2007) highlighted the influence of the homogeneous warming of the tropical SST, impacting upon the Sahelian drought through a warming of the free troposphere, affecting deep convection over Africa. Most of these results rely on “idealized” and “AMIP-like” experiments. The Atmospheric Model Intercomparison Project (AMIP) methodology consists in evaluating the atmospheric model performance and errors. In this framework, an ensemble of GCM simulations is carried out in which all members are forced by observed SST and sea-ice boundary conditions, each realization differing from the other by its imposed initial atmospheric conditions. Within the idealized framework, the model is usually forced by a specific SST anomaly pattern (warming of the Indian Ocean for example).

All these results are based on both “idealized” and “AMIP like” experiments in which each model has its own sensitivity, and consequently there is no real consensus on the mechanisms or basins responsible for the Sahelian drought. A difficult and additional question is the impact of human activities, or anthropogenic forcing. Can the Sahel drought be related to global climate change? As highlighted in Biasutti and Giannini (2006), the vast majority of the Coupled Model Intercomparison Project (CMIP3) models dry the Sahel in the late twentieth century when comparing historical experiments (in which observed anthropogenic forcings are applied) to pre-industrial runs. However, this does not mean that these models reproduce the 1970s–1990s drought and the associated underlying teleconnection mechanisms under realistic GHG and aerosols conditions. Indeed, considering the large panel of “state of the art” atmosphere-ocean coupled models (AOGCM) used in the Intergovernmental Panel on Climate Change (IPCC) AR4 report framework (through CMIP3), the large range of uncertainties present does not actually allow us to conclude on a preferred rainfall change scenario at the end of the twenty-first century over Africa (Joly et al. 2007; Douville et al. 2006).

Why is understanding climate change over Africa such a complex task? Rainfall variability over Africa is mainly driven by internal variability, linked to the strong coupling between land–ocean–atmosphere over this region. The difficulty arises from the different competing physical mechanisms that can lead to a precipitation decrease/increase at the end of the century over this region under enhanced greenhouse gases concentrations (see Table 1), and their representation in the AOGCM’s. An interesting mechanism linking Sahelian drought and the anthropogenic signal was proposed by Biasutti and Giannini (2006) and Held et al. (2005). The warming (cooling) of the Southern (Northern) hemisphere oceans after 1970, and consequently the Sahelian drought, could be linked to an asymmetric response of the SST to aerosols loading in the Northern hemisphere. This would tend, through solar radiation decrease, to counteract regionally the expected “uniform global” warming due to the greenhouse gases increase.

Table 1 Physical processes that can lead to a rainfall increase/reduction over the Sahel at the end of the twenty-first century under increased greenhouse gases and aerosols concentrations, according to previously published works

Sahelian rainfall increase	Sahelian rainfall decrease
A cooling (warming) of the southern (northern) hemisphere oceans	A warming (cooling) of the southern (northern) hemisphere oceans
Increased magnitude and frequency of the Niña events...	Increased magnitude and frequency of the Niño events...
Increased land ocean temperature contrast between the African continent and the Atlantic basin	A warmer Indo-Pacific, implying a more stable free troposphere
A warming of the Sahara leading to a deepening of the heat low	Desertification over the Sahel (Charney mechanism)
An increase in the water holding capacity of the atmosphere...	

However, this result should be interpreted with caution as it is model dependent. For example, while the CM2 GFDL/NOAA model simulates a significant drying at the end of the twenty-first century, partly related to strong model sensitivity to a uniform ocean warming, the NCAR model mainly simulates wet conditions over the Sahel, related to a deepening of the heat low (Haarsma et al. 2005).

The first objective of this work is to revisit the teleconnections between the different oceanic basins and sub-Saharan rainfall decadal to multi-decadal variability as simulated by a recent version of the ARPEGE model, and to highlight the physical mechanisms involved. The highlighted results would be compared to previously published ones in order to distinguish similarities and consensus across the different modelling studies.

The second purpose of this work is to extend this framework to the CMIP3 coupled models, both for the recent past (1950–1999) and the future (2050–2100). Namely, can we build a metric based on the accuracy of these models in both reproducing the observed sub-Saharan drought and the associated teleconnection mechanisms over the recent period (twentieth century) in order to improve our confidence in the twenty-first century climate projections over the Sahel?

In order to reach these objectives, the paper is presented as follows.

Section 2 briefly describes the model, the experimental setup and the selected observation data sets. Section 3 is devoted to the study of Sahelian rainfall variability at decadal to multi-decadal time scales over the second half of the twentieth century. This section is subdivided into three parts. First, a perfect model approach is considered to quantify the percentage of rainfall variability which is forced by the SST with respect to the internal variability of the atmospheric signal. Second, the accuracy of the ARPEGE model in reproducing the observed Sahelian drought is evaluated, based on ensemble simulations. Then, results from SST sensitivity experiments are investigated in order to determine the simulated physical mechanisms associated with the drought. In Sect. 4 the accuracy of the CMIP3 models in reproducing the observed Sahel drying and associated key mechanisms is investigated in order to determine the reliability of the twenty-first century scenarios. Finally, the last section gives a summary and provides some perspectives.

2 Observation data set description, model and experimental design

2.1 The ARPEGE-climate atmospheric model

The AGCM used in this study is the fourth version of the ARPEGE-climate model jointly developed by Météo

France and the European Center for Medium Range Weather Forecasts (ECMWF). Since the first release of this model (Déqué et al. 1994), many developments have been included (Déqué 1999). The model uses a two time level semi-lagrangian numerical scheme with a 30 min time step. There are 31 vertical levels, and the basic spectral truncation is T63. The physical package includes the turbulence scheme of Louis et al. (1981), the statistical cloud scheme of Ricard and Royer (1993) and the mass flux convective scheme of Bougeault (1985). The radiative forcing, including the effect of four GHG (CO₂, CH₄, N₂O and CFC) in addition to water vapour, ozone and of five aerosol types (organic and black carbon, sea salt, desert dust and sulphates) is computed by the Morcrette scheme (Morcrette 1990), which is activated every 3 h. At the surface, the interaction soil biosphere atmosphere (ISBA) land surface scheme (Noilhan and Planton 1989) is used to provide boundary conditions for the computation of surface fluxes (Mahfouf et al. 1995). A four layer heat diffusion scheme is used, and the soil hydrology representation holds four reservoirs: canopy interception, snow, shallow surface and root layer reservoirs [see Douville (2003) for a detailed description of ISBA].

2.2 Experimental design

An ensemble of 19 simulations was performed over the period 1950–1999. Within each ensemble, the simulations only differ by their initial atmospheric conditions. This ensemble (henceforth referred to as SSTFi) is forced by observed monthly SST (Smith and Reynolds 2004) and sea ice concentration time evolution, the greenhouse gases and sulphate (SUL) concentrations are held constant to their pre-industrial values (1900). The others aerosols (carbon, sea salt and desert dust) are kept constant and the indirect effect of the sulphate aerosols is not implemented in the model. As the observed SST are applied as lower boundary conditions to the atmospheric model, natural and anthropogenic external forcing are partly included in the forcing. The SSTFi ensemble mean gives an estimator of the atmospheric signal that is forced by the SST; and henceforth it will be referred to as SSTF. The deviation of each simulation from the mean provides an indication of the internal variability of the atmosphere as simulated by the model.

2.3 Observation data set

In order to highlight the model performance in reproducing the present climate variability over Africa several observation data sets are examined.

Simulated precipitations over Africa are compared to the global 0.5° × 0.5° resolution CRUTS2.1 data set (from the

Climatic Research Unit) for the period 1950–1999 (Mitchell and Jones 2005). Observed monthly sea surface temperatures (SST) used as boundary conditions for the AGCM are derived from the ERSSTv2 data set (Smith and Reynolds 2004).

3 Sahelian decadal variability as simulated by the ARPEGE GCM

3.1 SST forced versus the internal variability of the atmosphere over Africa

Quantifying the contributions to atmospheric variability by external forcing and internal dynamics is assessed using the analysis of variance often referred to as ANOVA technique and widely discussed in the literature (Zwiers 1996; Rowell and Zwiers 1999, among others). This statistical tool is based in its simplified form on the partition of the total variance of a given field into two independent components. For a given atmospheric variable, the total variance is partitioned by the externally forced variability (associated with the prescribed SST boundary conditions) and the internal variability (chaotic) generated by the model. The ratio of these two variance components is often referred to as potential predictability (PP hereafter). Many assumptions are needed in order to perform such variance decomposition. Indeed, the interaction between internal and externally forced variability is generally neglected in the ANOVA framework. Moreover, due to the finite number of ensemble members, the externally forced variability of the atmosphere is only approximated in the model's world. In the following, a raw (Fig. 1a) and spectral (Fig. 1b) analysis of variance were applied to the SSTFi ensemble in order to characterize the fraction of the rainfall variance due to the SST forcing. This was investigated during boreal summer (from July to September or JAS) over the 1951–1999 period. For more details about the assumptions, the algorithm and the significance test employed in the ANOVA framework, the reader is referred

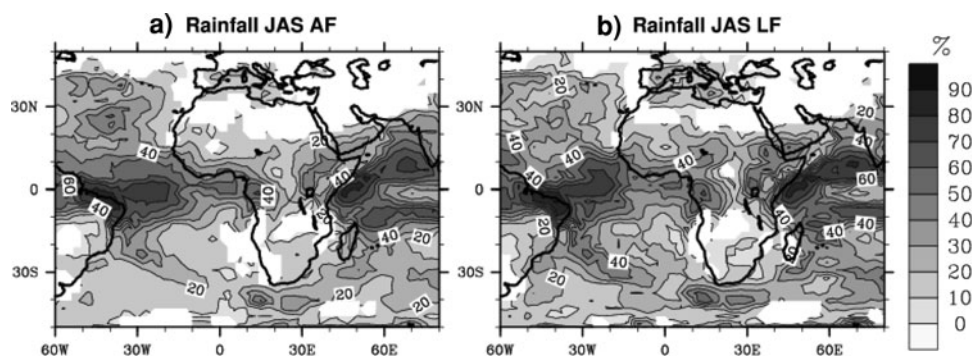
to Zwiers (1996) for the raw analysis and to Rowell and Zwiers (1999) for the spectral analysis.

The rainfall PP (Fig. 1a) is relatively high (60–70%) over the tropical Atlantic and Indian Ocean (marine ITCZ location). Here, the convection over the ocean can be interpreted as a direct response to the imposed SST anomaly. Focusing on the African continent, the PP is moderate (about 30–40%) over the western coast of Senegal, the gulf of Guinea, the Cameroon coasts and eastern Africa (Ethiopia). Conversely, the signal to noise ratio is low over the Sahel, where only 10–15% of the variance is due to the SST forcing. At decadal to multi-decadal time scales (Fig. 1b), the spatial pattern of PP is not clearly modified, but the amplitude is significantly increased. For example, the potential predictability increases from 10 to 15% (raw data) to 25–30% (low frequency filter) over the Sahel. Hence, this result indicates that for the African continent, the part of the rainfall signal imposed by the oceanic boundary conditions is increased at decadal to multi-decadal time scales. This result is consistent with other studies (Rowell and Zwiers 1999) which have suggested that the percentage of total variability forced by the SST tends to increase as longer timescales are considered. Here, the same analysis performed for the other seasons revealed that the PP over Africa is the highest during boreal summer (JAS, not shown).

However, the highlighted ANOVA results are based on “AMIP-like” climate simulations and therefore do not give an indication of the realism of the simulated variability, since in this “perfect model approach” the PP is only estimated in the model's world. Moreover, these results depend on ensemble size and rely on the assumption that there is no interaction between the SST forced and the internal variability of the atmosphere.

To go further, an analysis similar to the one used by Mehta et al. (2000) was performed to determine the number of simulations needed to correctly estimate the SST-forced signal, and to assess the model performance in terms of the simulated PP, over the Sahel. A Sahelian rainfall index (SRI) was first calculated for both the observations

Fig. 1 **a** Percentage of the variance of rainfall (unfiltered data) due to the SST forcing over the period 1951–1999 (JAS). *White areas* show no significant values with a *F* test at the 99% confidence level. **b** Same analysis performed at decadal time scale (8 year low pass filtered data)



(CRUTS2.1) and for each simulation of the SSTFi ensemble over the domain 16°W–45°E/10°N–20°N, over the 1950–1999 period during JAS. Groups of simulated SRI realizations were then averaged to reduce the internal variability of the atmospheric signal; each group ranging from 1 to 19 realizations of the climate system. These group-averaged simulated SRI were then used to perform correlation coefficients with the observed SRI. All the possible combinations of realizations were included in the calculation. Correlation coefficient as a function of the number of simulated SRI averaged in a group is displayed for both unfiltered and low pass filtered (with an 8 year cut-off) data in Fig. 2.

For a given group, the vertical bar indicates the correlation spread (min–max) and the curve represents the mean correlation coefficient. The raw averaged correlations for a given group range between 0.5 for two realizations to about 0.7 for 19 realizations, the best estimator of the SST forced signal. If the number of the ensemble size is small ($n = 2$ for example) the correlations range from approximately 0.3 to almost 0.7, and in this case the number of simulation used to compute the average is not sufficient to remove the internal variability. The correlation spread is significantly reduced for about ten realizations. This indicates that, for

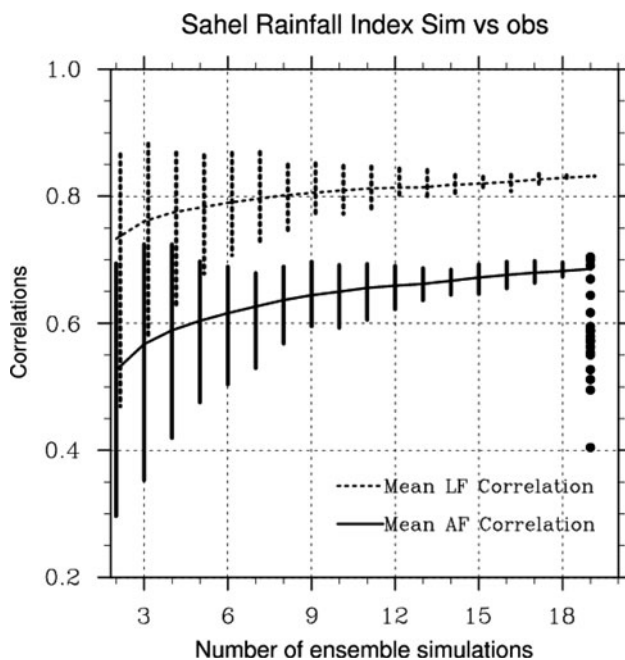


Fig. 2 Correlation coefficients between the observed (CRU data set) Sahelian Rainfall Index (SRI) and a simulated SRI averaged from various combinations of the 19 AGCM experiments; the vertical bar denote correlation coefficients calculated using unfiltered data (solid line) and low-pass (using an 8 year cut-off) filtered data (dashed), each curve represents the average correlation coefficients. Black dots denote correlation coefficient between each simulated SRI and the average of the remaining 18 simulated ones. See the text for more details

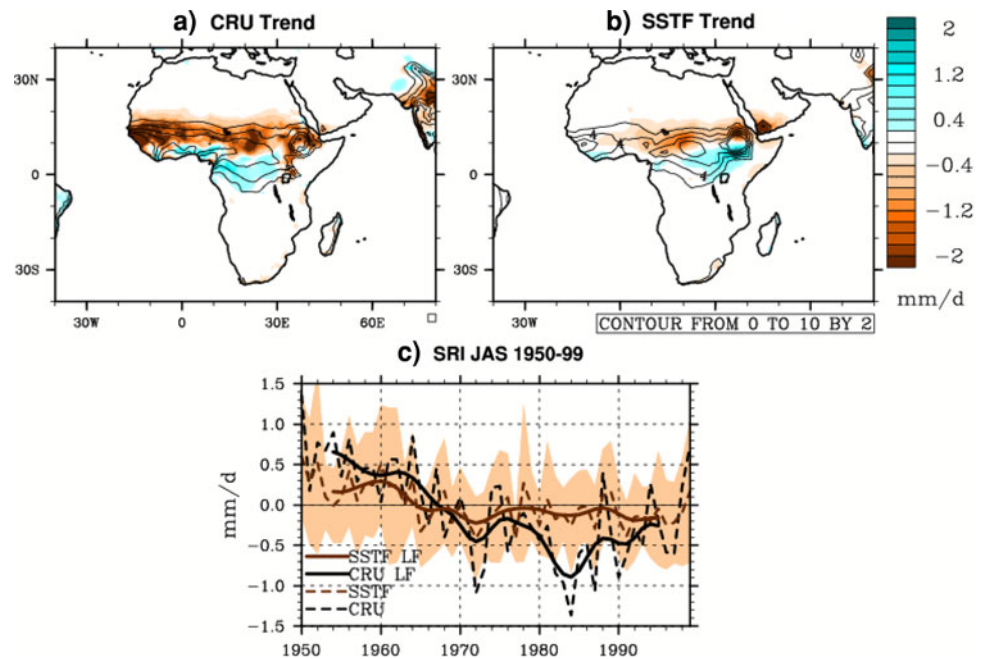
the ARPEGE model, the impact of SST upon rainfall variability within the “ensemble methodology” framework can be characterized with reasonable confidence if at least ten simulations are performed. At decadal time scale (Fig. 2, dotted line), the correlation plot is quite similar, except for a shift in the correlations to higher values. For the ensemble of all 19 realizations, the mean correlation coefficient increases from 0.7 (unfiltered data) to almost 0.85 at decadal time scale and lower. In other words, the 19-member ensemble mean explains approximately 50% (72% at decadal time scale) of the rainfall variance in nature’s single realization. In order to compare these results with the low frequency SRI variations generated by noise in the ARPEGE GCM, correlation coefficients were computed between each simulated SRI and the mean of the remaining 18 (Fig. 2, black dots). The 19 member ensemble mean explains about 50% of the observed rainfall variance, whereas it only explains 30% of its own realizations (the median correlation is about 0.55, see the black dots). This could imply that the model produces too much internal variance with respect to the observations. However, this result should be interpreted with caution because of the spread in the correlations (the black dots range correlation values between 0.4 and 0.7). Moreover, this analysis mixes the model skill (correlation) and the signal to noise ratio concept estimated within the ensemble methodology.

In summary, based on the ANOVA results, the simulated sub-Saharan rainfall variability seems to be mainly driven by the internal variability of the atmosphere. Nevertheless, the signal to noise ratio significantly increases during the establishment of the monsoon and at decadal to multi-decadal time scales. It is suggested that ten realizations of the climate system are required in order to correctly estimate the rainfall signal forced by the SST over Africa within the ensemble methodology framework. The next section will focus on the sub-Saharan decadal to multi-decadal variability as found in the observations and as simulated by the ARPEGE AGCM.

3.2 Simulated and observed sub-Saharan rainfall variability at decadal to multi-decadal time scales

The observed mean summer precipitation pattern associated with the African monsoon is distributed on a wide latitude band from 5°S to 18°N (JAS ITCZ location) and high precipitation areas are confined over the coast from Senegal to Liberia, downstream the Cameroon mountains and over the high plateau of Ethiopia (Fig. 3a, black contours). The rainfall pattern is well reproduced in the simulation, despite a clear overestimation of precipitation over the Ethiopian plateau, contrasting with an underestimation over the observed western coastal high precipitation

Fig. 3 Linear trend of JAS summer precipitation from 1950 to 1999 estimated from **a** CRU observations and **b** SSTF ensemble mean. Unit is mm/day/50 years, and the associated climatology is depicted by the *black contours*. **c** Sahelian rainfall index (10°N – 20°N , 16°W – 45°E) anomaly (vs. the 1950–1999 mean) calculated for both observations and SSTF (*dashed lines*). The *filled area* highlights the spread (defined as the minimum and maximum of the 19 simulations with respect to the ensemble mean) in the SSTFi ensemble. The *solid line* depicts that an 8 year low pass filter has been applied to the time series



areas (Fig. 3b). These biases are common to other models, and are consistent with the coarse orography representation in current state of the art AGCMs. Considering the mean large scale dynamic, the Saharan thermal low is well simulated by the model, the Tropical Easterly Jet's (TEJ) westward extension is underestimated over the African continent, and the simulated African easterly jet (AEJ) is weaker and its latitudinal extension is wider than the observed one during boreal summer (not shown). Despite these model biases, the mean features of the African monsoon are reasonably well reproduced by the ARPEGE AGCM.

Figure 3a shows the spatial pattern of the linear trend in observed summer precipitation over the period 1950–1999. A significant drought (with rainfall reductions of 20–50%) is depicted over the whole Sahelian band, contrasting with a slight precipitation increase over the Gulf of Guinea. Rainfall variability over the Sahel is characterized by a wet period occurring from 1950 to 1970 which contrasts with a persistent period of desiccation from 1970 to 1990, followed by a partial recovery during the last decade of the twentieth century (Fig. 3c, solid black line). The linear trend in precipitation, as simulated by the model ensemble mean (SSTF), exhibits a dipolar pattern, contrasting a rainfall increase over the central and eastern part of the Sahel (from Niger to Sudan) with wetter conditions over northern Ethiopia and southern Sudan (Fig. 3b). Nevertheless, the observed drought over West Africa and the wetting over the Gulf of Guinea are not captured by the model. Moreover, the drought signal over central and eastern Africa is underestimated. It seems that the simulated rainfall trend pattern is shifted eastward compared to

the observed one. The simulated SRI (SSTF) is able to reproduce the observed rainfall variability at decadal to multi-decadal time scales despite a clear underestimation of its magnitude (by about a factor 3), and the failure in capturing the 1990s recovery (Fig. 3c, solid brown line). Moreover, there is a strong underestimation of the 1980s observed drought (simulated negative anomalies remain more or less constant over the 1970–1990 period). The correlation between the observed and simulated SRI is about 0.68 (0.83) for unfiltered (filtered) data. A strong contribution of the atmospheric internal variability in driving the simulated rainfall variability over the Sahel is also indicated by the significant spread on Fig. 3c. These results are consistent with a principal component analysis applied to the observations and to SSTF (not shown). The spatial linear trend patterns previously described are quite similar to the first leading mode pattern for the observations (explaining 28% of the total variance) and the second mode for SSTF (14% of explained variance). The associated principal components (time series) are close to the SRI displayed on Fig. 3c.

In previous studies, this observed dipolar rainfall pattern has often been associated with a southward location of the ITCZ (and thus the Hadley Cell southern branch); a southward displaced and intensified AEJ, a weakened TEJ that does not extend as far south, and decreased vertical motion over the Sahel (Grist and Nicholson 2001; Fontaine and Janicot 1992). In SSTF, the dipolar rainfall pattern is clearly consistent with a southward displacement of the rainbelt over central and eastern Sahel, the Harmattan winds and the monsoon flow convergence area is shifted about 2° southward during the drought, but no clear AEJ and TEJ

modification (unrealistic decoupling between the dynamical jets and the rainfall at the surface). For both the ensemble mean and the observations, the SRI is significantly correlated with an inter-hemispheric SST pattern at global scale (Fig. 4). The transition between the observed wet and dry period is associated to a reversal of the SST anomalies, the southern (northern) oceans warmed (cooled) after 1970. This mode known as “the inter-hemispheric SST mode” is characterized by a dipolar pattern over the Atlantic basin (Atlantic dipole), a warming of the Indian Ocean and the tropical Pacific after 1970, and a pattern similar to the Pacific decadal oscillation (PDO) in the northern Pacific (Fig. 4a). The observed correlation pattern is close to the simulated one (Fig. 4b) despite slight regional differences over the tropical Pacific and the Atlantic.

In summary, the analysis of the ARPEGE GCM ensemble simulations has confirmed that the basic structure of the Sahel drought can be simulated when the model only uses the observed SST as lower boundary conditions. However, the simulated precipitation decrease is mainly located over central and eastern Sahel and underestimated. Furthermore, the decadal to multi-decadal rainfall variability over the sub-Saharan region mainly arises from atmospheric internal processes.

The simulated rainfall trend is associated to a southward shift of the Sahelian rainbelt, and is significantly linked to an inter-hemispheric SST pattern at global scale. Note also that another simulation ensemble has been performed with ARPEGE in which we prescribe evolving greenhouse gases and sulphate aerosols atmospheric concentrations. In this ensemble simulation, the West African monsoon system is not significantly modified with respect to the SSTFi ensemble. As observed SSTs are prescribed in both ensembles, all natural and anthropogenic forcings are already included in the SST signal. However, enhancing GHG and sulphate concentration in the atmosphere leads to a significant diurnal temperature range decrease during the last two decades of the twentieth century over the African continent (Caminade and Terray 2006).

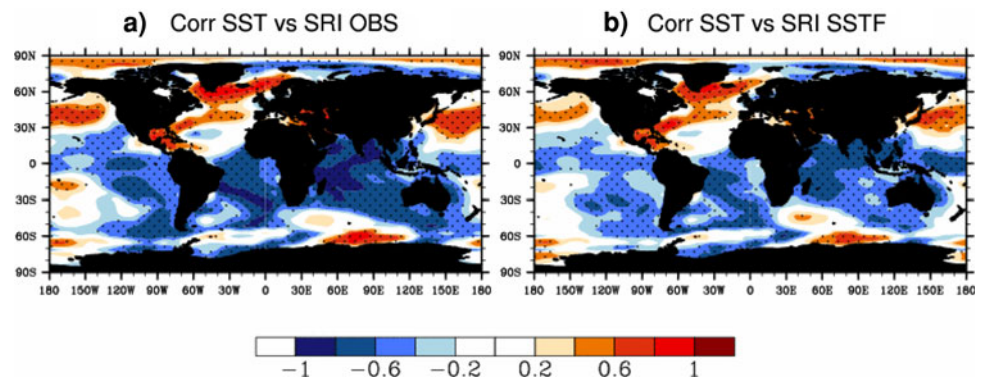
In this section we have not considered the physical mechanisms responsible of the rainfall changes or quantified the respective role of the different oceanic basins. In the next section, a methodology similar to the one used in previous studies (Palmer 1986; Folland et al. 1986; Lu and Delworth 2005) is applied to determine the role of the different basins in driving the drought as simulated by the ARPEGE AGCM, and to compare its response to other model’s results.

3.3 Respective role of the different oceanic basins in driving the simulated Sahel drought

3.3.1 Methodology and experimental design

In order to estimate the role of the different oceanic basins in driving the sub-Saharan rainfall trend, several ensembles of idealized experiments were performed. A first ensemble of 20 simulations was forced by the mean (1950–1999) seasonal cycle of SST and sea ice concentrations (Smith and Reynolds 2004). Each realization differs from the others by its initial atmospheric conditions. The ensemble mean, which will be the “reference” control experiment in this study, will be referred hereafter as to CTL. In the second ensemble, the SST forcing was computed as the sum of the mean seasonal cycle plus an anomaly, at global scale. The associated ensemble mean will be denoted as to GLOB. This anomaly was computed as the linear regression between global summer SST and the SSTFi simulated SRI at decadal and longer time scales. This SST inter-hemispheric pattern is shown on Fig. 5. The difference between GLOB and CTL was investigated for the summer season, to characterize the ARPEGE atmospheric model sensitivity to the global inter-hemispheric SST mode. In order to determine the influence of each oceanic basin upon sub-Saharan rainfall, three additional ensembles were performed in which the SST anomaly was only prescribed over the Indian, the Atlantic and Pacific basins (see Fig. 5 for a definition of the selected geographical domain). The

Fig. 4 Spatial correlation between observed Sea surface temperature (ERSSTv2 data set) and the SRI (JAS 1950–1999) for both CRU observation (a) and the SSTFi ensemble mean (b). The data have been low pass filtered with an 8 year cut-off. The dotted area denotes significant correlations at the 5% significance level as estimated by a student *t* test



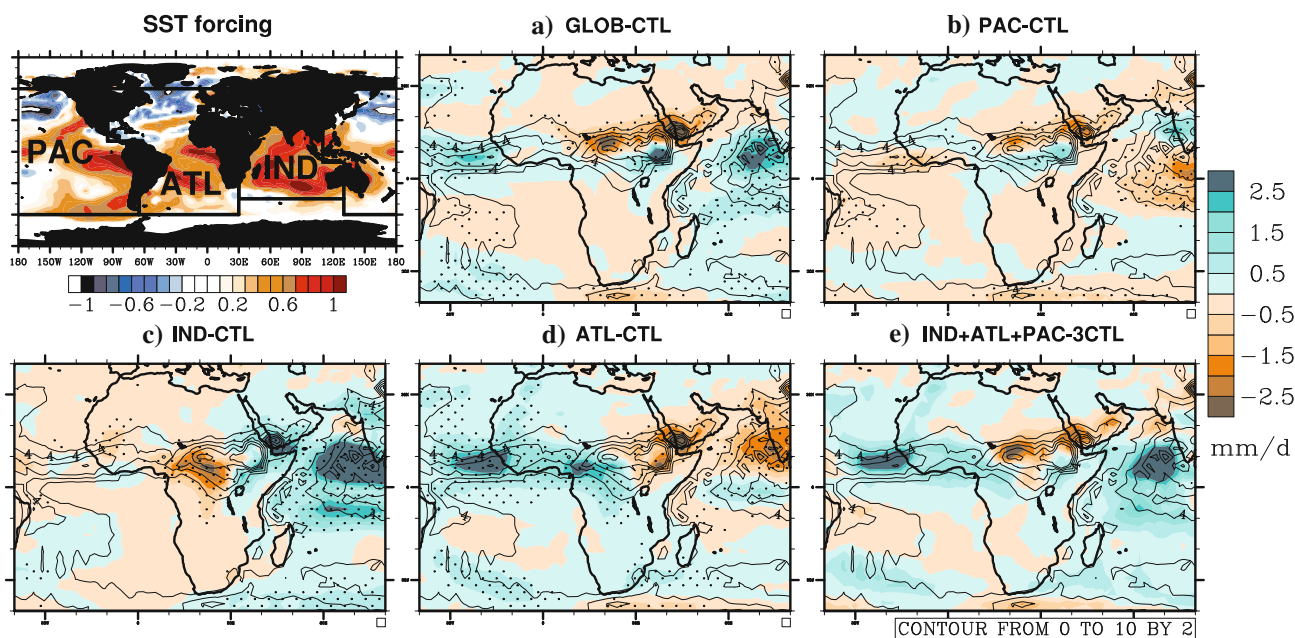


Fig. 5 Left upper view: regression pattern of JAS summer SST during 1950–1999 against the simulated SRI (SSTF). The data have been low-pass filtered (8 year cut-off) and the amplitude has been scaled to correspond to the trend during 50 years (unit: K/50 years). **a–e** Summer African rainfall response to SST forcing in different

idealized experiments (see the text for more details). The CTL climatology is depicted by the *black contours*. The *dotted area* denotes significant changes at the 5% significance level as estimated by a student *t* test

associated ensemble means will henceforth be denoted as IND, ATL and PAC, respectively.

3.3.2 Rainfall response

The simulated summer rainfall response in the GLOB experiment (Fig. 5a) is similar to the SSTF ensemble mean trend previously described (Fig. 3b), depicting a meridional dipolar pattern over the central and eastern Sahel. Nevertheless, the magnitude of the response in GLOB is somewhat larger, and the pattern is slightly shifted northward compared to the SSTF trend, due to the mean ITCZ location in CTL. Furthermore, combining the response in ATL, IND and PAC (Fig. 5e) reproduces the rainfall response as simulated in GLOB experiment, with only slight regional differences. This provides a validation of the experimental design and also confirms the use of these idealized experiments in comparison with the realization of costly “AMIP-like” ensembles.

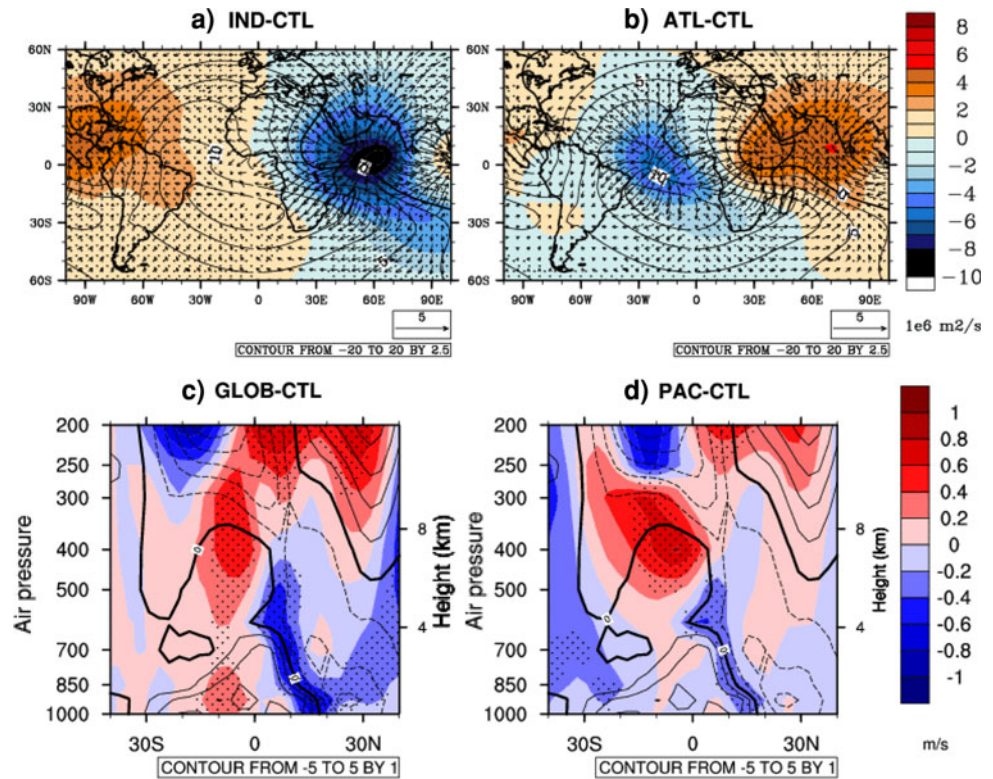
The rainfall response in GLOB confirms the importance of the inter-hemispheric SST mode in driving the Sahelian desiccation. However, the simulated drought signal is restricted over central and eastern Sahel. Now considering each basin separately, the simulated African rainfall response to the Pacific SST forcing (Fig. 5b) consists of a meridional rainfall dipole relatively similar to that found in GLOB. In ATL (Fig. 5d), the rainfall anomaly pattern contrasts a precipitation increase over the western coasts

(Guinea coast) and the centre (Cameroon) of Africa with a decrease over the eastern region (Sudan), the Arabic peninsula and the Indian basin. The rainfall response associated with the warming of the Indian basin (Fig. 5c) is almost the opposite of ATL, and is characterized by a rainfall increase (decrease) over the Indian Ocean and eastern (central) Africa. It is quite a surprising result that the ATL and IND rainfall anomaly patterns are zonal dipoles whereas they are meridional ones for both GLOB and PAC experiments. Moreover, the effects of the Atlantic and Indian basins seem to compensate regionally over central and eastern Sahel, suggesting the Pacific Ocean is the preponderant driver of the simulated sub-Saharan rainfall trend (in ARPEGE).

3.3.3 Teleconnection mechanisms

The simulated rainfall response in IND and ATL can be related to a modification of the zonal circulation over the Indo-Atlantic basin (Fig. 6a, b). The warming of the Indian SST leads to upper tropospheric (at 200 hPa) divergence over the Indian basin and enhanced convergence over Central America (Fig. 6a), and the inverse at low levels (850 hPa, not shown). The convection is thus enhanced leading to increased rainfall over the Indian basin and eastern Africa and decreased rainfall over central Africa due to orographic conditions. Indeed, the negative rainfall anomalies for the IND experiment are restricted to the

Fig. 6 Upper views 200 hPa potential velocity (*shading*) and divergent winds (*vectors*) responses in IND (a) and ATL (b) experiments. Lower views meridional wind response (averaged between 0° and 45°E) in GLOB (c) and PAC (d) experiments. The CTL climatology is depicted by the *black contours*. The *dotted area* denotes significant changes at the 5% significance level as estimated by a student *t* test



Congo basin and the Chad. This area is surrounded by natural mountains. The comparison of evaporation and moisture convergence anomalies highlights the importance of dry advection over this area, consistent with a downhill Föhn effect (not shown).

In response to the Atlantic SST forcing, a direct Walker cell type anomaly develops, which ascends over the tropical Atlantic Ocean and descends over eastern Africa and the Indian basin (Fig. 6b). This modification of the zonal circulation is consistent with the simulated rainfall anomaly zonal dipole in ATL: increased convection over the western coasts of Africa and enhanced subsidence over eastern Africa.

In contrast, the meridional rainfall response in the GLOB and PAC experiments is mainly due to a southward shift of the rainbelt over central and eastern Sahel (Fig. 6c, d). For both experiments, the convergence zone between the dry Harmattan winds and the monsoon flow at the surface, and the upper tropospheric divergence area, is clearly shifted southward. Thus, this result is consistent with a southward displaced Hadley cell convergence area, leading to a meridional rainfall anomaly pattern.

To further interpret the Sahel drying signal in PAC experiment, we analysed the mean tropospheric temperature (hereafter TT) response to the prescribed SST forcing (Fig. 7). In response to the prescribed SST inter-hemispheric pattern, the troposphere warms up over the entire tropical band and over a vast area of the southern

hemisphere whereas it cools over the high latitudes of the northern hemisphere (Fig. 7a). The mean tropospheric temperature significantly increases over the entire tropical belt in PAC (Fig. 7b). This tropical TT warming is similar to the first leading EOF mode in the SSTF ensemble mean at decadal and lower time scales (Fig. 7c). In the ATL experiment, the TT warms up over the Gulf of Guinea and the tropical Atlantic Ocean (not shown). There is also a large TT increase over central/eastern Africa and the Indian Ocean in IND.

A mechanism relating dry events over the Sahel and TT warming has already been shown in previous studies focusing on the El Niño impact upon tropical rainfall at interannual time scale (Yulaeva and Wallace 1994; Chiang and Sobel 2002; Su et al. 2005). The warming of the tropical Pacific leads to a homogeneous warming of the free troposphere over the whole tropical band. This warming causes the stabilization of the atmosphere through a stabilization of the vertical profiles of equivalent potential temperature (θ_e) at low levels, leading to a reduction of deep convection over the tropics and thus a reduction in precipitation. Furthermore, the TT warming has been recently argued to be (at least in part) a plausible cause of the Sahel drying at decadal time scale (Herceg et al. 2007). As highlighted in the work of Herceg et al. (2007), if the TT warming can be partly responsible for the Sahelian rainfall decrease, the physical mechanisms involved must surely be more complex.

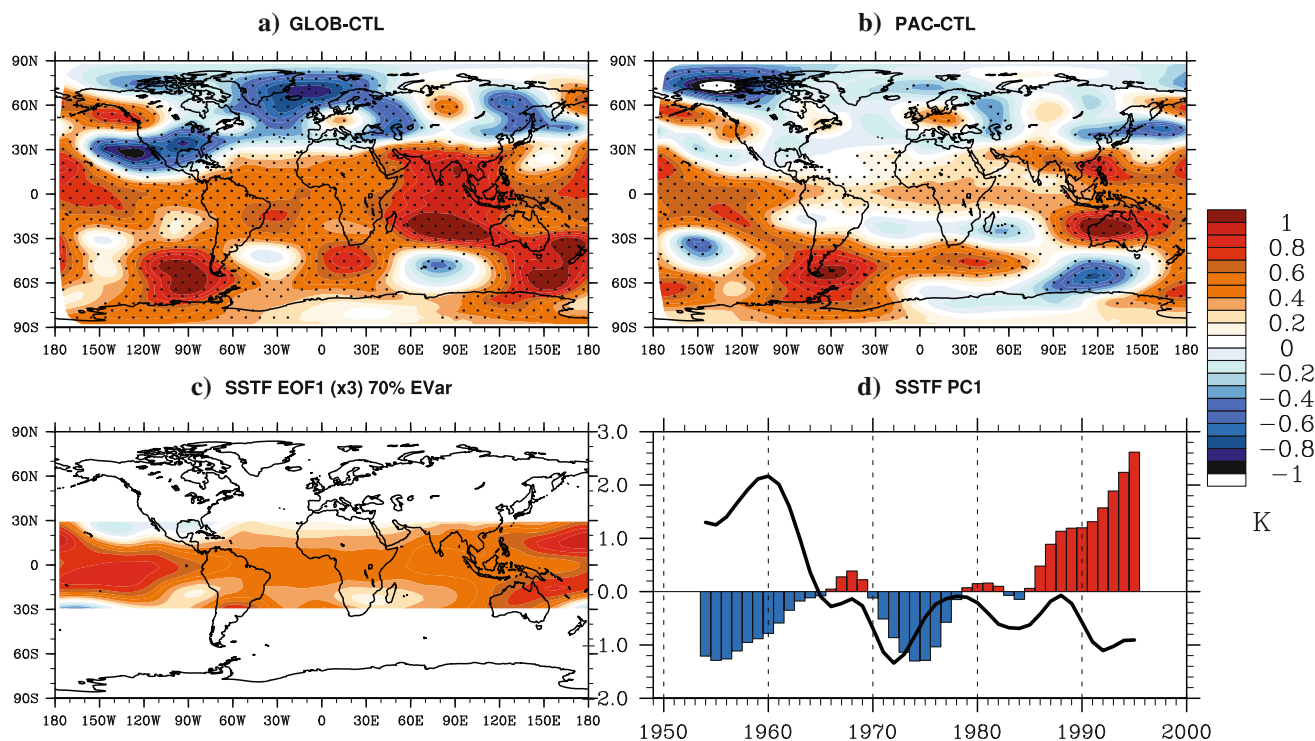


Fig. 7 Upper views mean tropospheric temperature (weighted average between 300 and 700 hPa) response in GLOB (a) and PAC (b) experiments. The dotted area denotes significant changes at the 5% significance level as estimated by a student *t* test. Lower views c spatial patterns associated with the first mode of a principal

component analysis applied to the SSTF mean tropospheric temperature. A factor three has been applied for visualization commodities. The data have been first low-pass filtered with an 8 year cut-off. d Associated normalized principal component (bar). The black curve depicts the simulated normalized SRI in SSTF

First, the expected anti-correlation between the simulated SRI and the principal component associated with the low-frequency TT mode is not consistent during the 1970s (Fig. 7d). This mismatch invalidates the TT mechanism for this period in the AMIP-like ensemble. The linear approach employed in the “idealized experiment” section is obviously limited (an anomaly pattern is applied, so there is no SST variability in these experiments, conversely with the SSTFi ensemble). Perhaps during the 1970s (when the mismatch occurs) another mechanism is active in the model ensemble simulation.

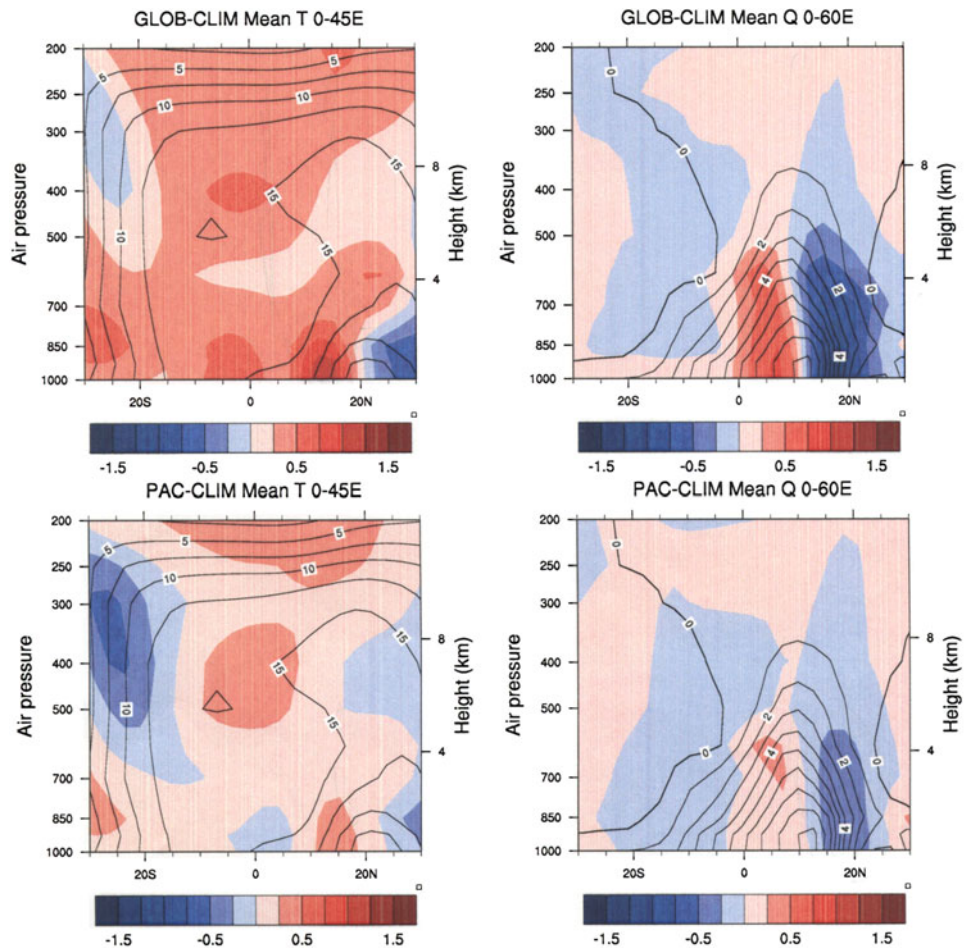
Then, the TT warming is expected to reduce deep convection over the entire tropical band. It should lead to a uniform rainfall decrease over Africa, and not to a simulated meridional rainfall anomaly pattern as highlighted in GLOB and PAC. Note also that the stabilization mechanism is not really active in ATL, as the surface has already equilibrated to warmer temperature (not shown). In IND, the large TT increase over central and eastern Africa is not fully compensated by the surface warming. This means that the stabilization mechanism is slightly active here, its effect superimposing on zonal circulation anomalies (not shown).

Thus, the rainbelt shift shown in the PAC experiment cannot be directly related to a stabilization of TT by itself.

The proximate causes of the drying certainly involve more subtle feedbacks, such as described by Neelin et al. (2003) and Chou and Neelin (2004). Indeed, an indirect effect of the temperature stabilization consists in enhanced dry advection from non-convective regions (here the Sahara) to the margin of convective zones (the Sahel). For this mechanism referred to as the “upped ante mechanism”, the warming of the free troposphere increases the value of surface boundary layer moisture required for convection to occur. For regions in which moisture supply is high, moisture increase is required to maintain the occurrence of precipitation, but this increases the moisture gradient relative to neighbouring subsidence zones. This results in rainfall reduction over those margins of convection zones which have a strong inflow of air from subsidence areas (the conditions to deep convection to occur are less frequently met). Neelin et al. (2003) shows that this mechanism is the leading cause of tropical drying in global warming experiment, in which the surface is expected to warm first, and could be dominant for specific areas during El Niño events.

Figure 8 displays the temperature and relative humidity vertical profile anomalies for both PAC and GLOB experiments. Between 0°N and 10°N (positive rainfall anomalies zone), the boundary layer temperatures are

Fig. 8 *Left* temperature response (averaged between 0° and 45°E) in GLOB (*upper view*) and PAC (*lower view*) experiments (unit: K). *Right* relative humidity response (averaged between 0° and 60°E) in GLOB (*upper view*) and PAC (*lower view*) experiments (unit: g/kg). The CTL climatology is depicted by the *black contours*



slightly lower than the ones in the free troposphere. The relative humidity is enhanced in both experiments, but is relatively weak for the PAC experiment. Over the dry area (eastern part of the Sahel), namely between 10°N and 20°N, the boundary layer is warmer than the free troposphere, and relative humidity decreases. As the boundary layer is warmer than the free troposphere here, deep convection should be enhanced, but as the moisture supply significantly decreases at the edge of the convection zone, it leads to decreased precipitation over this area. These features fit the upped ante mechanism. Note also that, in equilibrium, the simple TT stabilization is not really active in GLOB and PAC.

Other sensitivity experiments should be carried out with the ARPEGE AGCM to precisely show how the TT anomaly propagates and interacts with deep convection regionally over sub-Saharan Africa. More detailed companion analysis must be carried out as well, such as construction of moist static energy budget, in order to check if the “upped ante” feedback is really active in the model.

Here, we just suggest the possible contribution of the Pacific in partly driving the simulated Sahel drought, via

the tropical warming of the free troposphere and especially the “upped ante” mechanism previously described.

3.4 Discussion

The experimental design employed in this study is similar to that of Lu and Delworth (2005). However, although the SST forcing is relatively similar, Lu and Delworth showed an impact of both the Pacific and the Indian basin upon the Sahel drought as simulated by the GFDL AM2 model. Hoerling et al. (2006) highlighted the influence of the Atlantic basin in driving the drought (the influence of the Indian basin resulting in little precipitation change over the Sahel) whereas the works of Bader and Latif (2003) suggested the preponderant effect of the Indian basin using the ECHAM model. Despite the different model sensitivities, the Sahelian drought is captured when the atmospheric model is forced by the observed global SST. This feature is relatively robust across all related modelisation studies.

One should question the realism of the ARPEGE model sensitivity to the Atlantic SST dipole, compared to previously published results. Indeed, the rainfall anomalies

displayed in ATL-CTL exhibit a zonal dipole pattern whereas a southward location of the ITCZ (and thus a meridional rainfall anomaly pattern) is associated with the Atlantic SST dipole in many studies (Hoerling et al. 2006). It could call into question the fidelity of the model in assessing the sensitivity of Sahelian rainfall to global SSTs. In fact, the model is really sensitive to the SST warming over the Gulf of Guinea, rather than the Atlantic SST dipole by itself. This leads to increased convergence (and precipitation) over West Africa and decreased convection over Eastern Africa. The simulated main mode of rainfall variability at interannual time scale (SSTFi ensemble) is relatively similar to the ATL-CTL experiment (not shown), and to some extent, is closed to the “Guinean” rainfall mode highlighted in Giannini et al. (2003). Moreover, the simulated mean rainfall bias exhibits the same pattern. The fact that dry anomalies in the SSTF ensemble mean (and in the GLOB experiment) do not extend over West Africa could probably be related to this feature. Namely, whatever the time scale considered, the simulated precipitation over West Africa are oversensitive to warm SST anomalies over the Gulf of Guinea. This bias could be amplified in global warming scenario simulations as the *cnrm_cm3* coupled model (in which the atmospheric component is ARPEGE) used in the IPCC AR4 framework fails in reproducing the Atlantic cold tongue, leading to a warm SST bias over the Gulf of Guinea (this feature is also common in most of the CMIP3 coupled models).

Anyway, sensitivity experiments show that the influence of a given basin is certainly model-dependent: the atmospheric model ensemble mean captures the Sahelian rainfall decadal variability, but surely for different physical mechanisms. Consequently, coordinated experiments must be carried out to characterize the Sahelian rainfall response to similar prescribed SST anomalies, for the largest set of available atmospheric models. This will be achieved within the African monsoon multidisciplinary analysis project framework.

Another problem comes from the difficulty to validate the mechanisms responsible for the Sahelian drought at multi-decadal time scales. Indeed, a limitation of the NCEP reanalysis in characterizing the low-frequency variability of the atmospheric circulation has been shown by Kinter et al. (2004) over the tropics, and more specifically over Africa by Camberlin et al. (2001) and Poccard et al. (2000).

Nevertheless, despite the spread in the simulated teleconnection mechanisms by different atmospheric models, and the difficulty of validating them by comparison with the reanalysis, a few consensus points have been corroborated by this work. First, an AGCM forced by prescribed SST time evolution is able to capture the sub-Saharan low frequency rainfall variability. The drought is linked with an

inter-hemispheric SST mode, and with a warming of the free troposphere over the Tropics. For the ARPEGE model, the Sahelian rainfall anomalies are mainly attributed to the Pacific SST, in agreement with the so-called “upped ante” mechanism highlighted in the works of Neelin et al. (2003).

In the real world, one could wonder the relative importance of the global/Atlantic gradient (with high loadings in the extra-tropics) and the tropical warming (mainly Indian-Pacific) signal upon Sahelian rainfall variability at inter-decadal time scale and their inter-dependence as well. Even if our model results highlight the importance of the TT warming, we suggest that both effects could superimpose. The variability of the Pacific SST at inter-decadal time scale and its influence upon Sahelian rainfall must be further characterized. For example, companion AMIP-like ensemble experiments in which the SST variability will only be prescribed in the Pacific and over the Tropics must be performed to confirm these results. It could then confirm or invalidate the TT/SRI positive correlation values during the 1970s (mismatch previously noted on Fig. 7d).

Despite these caveats, and relying on the “multi-model consensus”, we will focus on the simulated Sahelian rainfall variability and its link with both the interhemispheric SST mode and the TT for full coupled ocean-atmosphere models used in the IPCC AR4 framework (CMIP3). These links will be investigated for both the twentieth and the twenty-first centuries in the following section.

4 Sahelian decadal to multi-decadal variability and its link with global sea surface and tropospheric temperatures as simulated by the CMIP3 coupled models

4.1 Mean changes and multi-model spread

The coupled model integrations performed for the fourth assessment report of the Intergovernmental panel on climate change are examined. 21 models are investigated for both the twentieth century (20c3m in the following) and the twenty-first century projections, based here on the SRESA1B scenario integrations (SRESA1B hereafter). Concerning the 20c3m simulations, the coupled models are forced by the historical time evolution of greenhouse gases and sulphate aerosols emissions, and in few models by other anthropogenic (black carbon aerosols and vegetation/land use patterns) and natural (solar radiation, volcanic dust) forcings. The SRESA1B scenario relies on a growing world economy and advances in technology over the twenty-first century. It is translated in terms of emissions by a CO₂ concentration that reaches 720 ppmv in 2100 and

Table 2 List of the 21 coupled models and their relevant informations

Model	Modeling group and country	Atmosphere resolution	Ocean resolution	Forcings
bccr_bcm2_0	BCCR, Norway	2.81° × 2.79°	0.5–1.5° × 1.5°	G, SD
cccma_cgcm3_1	CCCMA, Canada	3.75° × 3.71°	1.85° × 1.85°	G, SD
cccma_cgcm3_1_t63	CCCMA, Canada	2.81° × 2.79°	1.4° × 0.9°	G, SD
cnrm_cm3	CNRM, France	2.81° × 2.79°	2° × 0.5°	G, O, SD, BC
csiro_mk3_0	CSIRO, Australia	1.88° × 1.87°	1.88° × 0.84°	G, O, SD
csiro_mk3_5	CSIRO, Australia	1.88° × 1.87°	1.88° × 0.84°	G, O, SD
gfdl_cm2_0	GFDL, USA	2.5° × 2°	1° × 1/3°	G, O, SD, BC, OC, LU, SO, V
gfdl_cm2_1	GFDL, USA	2.5° × 2°	1° × 1/3°	G, O, SD, BC, OC, LU, SO, V
giss_aom	NASA/GISS, USA	4° × 3°	4° × 3°	G, SD, SS
iap_fggoals1_0_g	LASG/IAP, China	2.81° × 3.05°	1° × 1°	G, SD
inmcm3_0	INM, Russia	5° × 4°	2.5° × 2°	G, SD, SO
ipsl_cm4	IPSL, France	3.75° × 2.54°	2° × 1°	G, SD, SI
miroc3_2_hires	CCSR, NIES, FRCGC, Japan	1.13° × 1.12°	0.28° × 0.19°	G, O, SD, BC, OC, MD, SS, LU, SO, V
miroc3_2_medres	CCSR, NIES, FRCGC, Japan	2.81° × 2.79°	1.4° × 0.5°	G, O, SD, BC, OC, MD, SS, LU, SO, V
miub_echo_g	MIUB/METRI/M&D, Germany and Korea	3.8° × 3.8°	T42 2.81° × 2.79°	G, SD, SI
mpi_echam5	MPI, Germany	1.88° × 1.87°	1.5° × 1.5°	G, O, SD, SI
mri_cgcm2_3_2a	MRI, Japan	2.81° × 2.79°	2.5° × 0.5°	G, SD, SO
ncar_ccsm3_0	NCAR, USA	1.41° × 1.4°	1.13° × 0.27°	G, O, SD, BC, OC, SO, V
ncar_pcm1	NCAR, USA	2.81° × 2.79°	1.13° × 0.27°	G, O, SD, SO, V
ukmo_hadcm3	UKMO, UK	3.75° × 2.50°	1.25° × 1.25°	G, O, SD, SI
ukmo_hadgem1	UKMO, UK	1.88° × 1.25°	1° × 1/3°	G, O, SD, SI, BC, OC, LU, SO, V

The acronyms depicting anthropogenic and natural forcings time evolution included in the historical integrations are the following: *G* well mixed GHGs, *O* ozone, *SD* sulphate direct effect, *SI* sulphate indirect effect, *BC* black carbon, *OC* organic carbon, *MD* mineral dust, *SS* sea salt, *LU* land use, *SO* solar irradiance and *V* volcanic aerosol

then stabilizes at this level, while sulphate aerosol decreases. Table 2 highlights an overview of the different model characteristics. Note that a detailed description of all models and integrations set-up is available at: http://www-pcmdi.llnl.gov/ipcc/model_documentation/ipcc_model_documentation.php

Considering mean rainfall changes (JAS) as simulated by the CMIP3 models at the end of the twenty-first century (Fig. 9), a wide range of scenarios for Africa are conceivable. Indeed, some models predict wet conditions over the continental Sahel (both version of *miroc_3_2* and *ukmo* models, *mpi_echam5*, *miub_echo_g*), some predict a rainfall decrease (*gfdl_cm2_0* and *gfdl_cm2_1*) while some do not show significant changes over continent, the mean precipitation change signal being located over the tropical Atlantic ocean or along the Guinea coast (*bccr_bcm2_0*, *csiro_mk3_0*, *inm3_0*, *ipsl_cm4*).

Moreover, the different scenarios exhibit both meridional dipole patterns, characteristic of a shift of the ITCZ (that can be northward, see *miroc_3_2_medres* as an example or southward, see *ipsl_cm4*) and zonal ones that can be suggested to be related to a modification of Walker

cell type circulation (*bccr_bcm2_0* and *cnrm_cm3* depicting a rainfall increase over the Guinea coast and a decrease over East Africa/Saudi Arabia).

As a consequence of the huge spread in the different model scenarios, rainfall changes as simulated by the multi-model ensemble mean have a limited meaning (Fig. 10a). If the ensemble mean predicts drier conditions over the Gulf of Guinea and the western coast of Mauritania, wetter conditions over the northern edge of Mali/Niger (and few grid points over Sudan), the change in the mean is about 1/4 compared to the spread (Fig. 10b) in the different rainfall scenarios (defined as one standard deviation of the different model projections with respect to the ensemble mean).

Thus, at this point, there is no clear consensus concerning the future rainfall mean changes over sub-Saharan Africa at the end of the twenty-first century.

A simple metric is defined to distinguish the ability of the CMIP3 coupled models in capturing the two main mechanisms described above which are related to the Sahelian drought during the observed period, and to highlight if these links remain unchanged for the future.

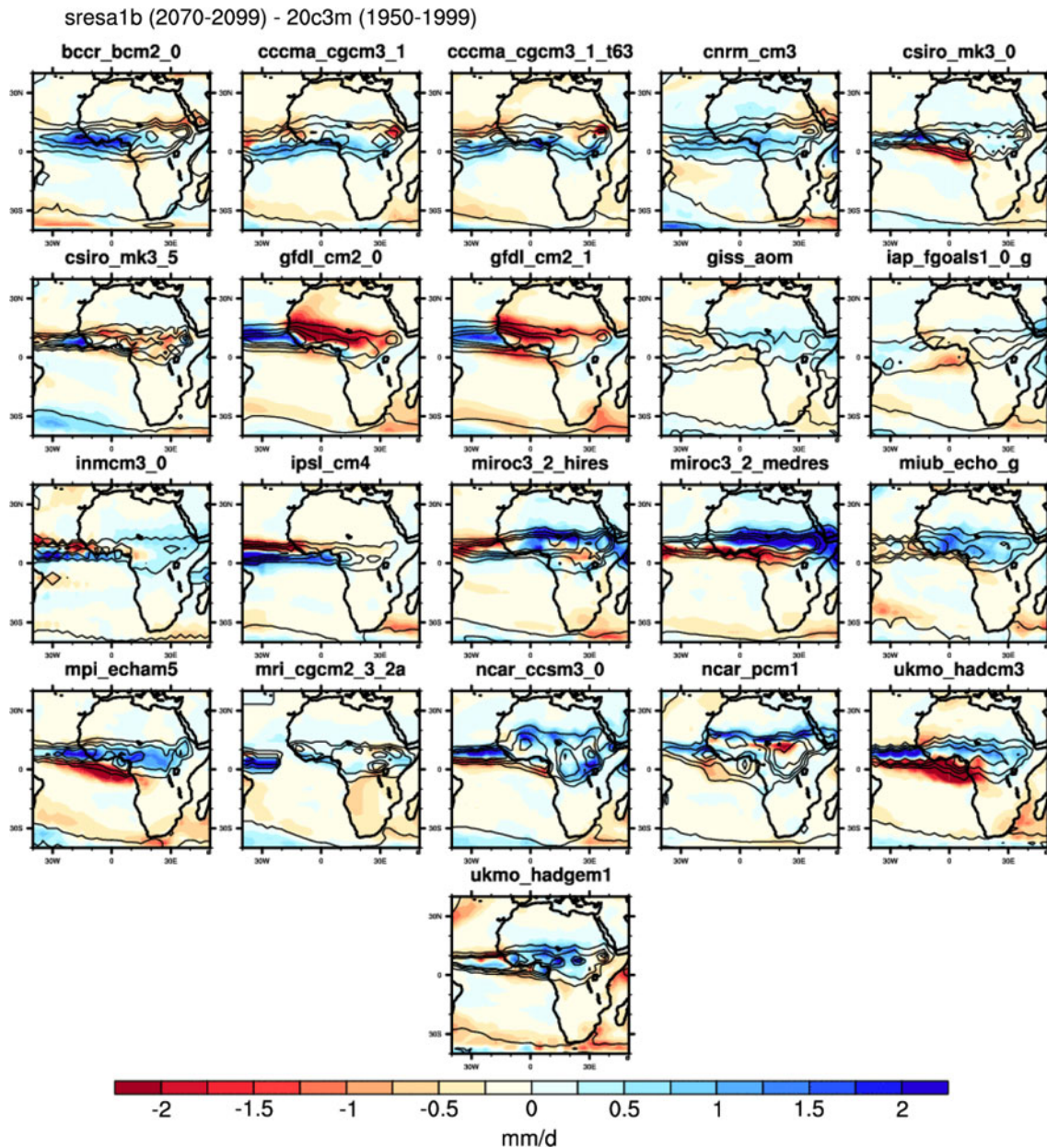


Fig. 9 Mean seasonal (JAS) rainfall changes (*shading*) as simulated by different coupled models from the CMIP3 AR4 database. The difference is computed between the time windows 2070–2100

(SRESA1B emission scenario) and 1950–1999 (historical experiment 20c3m). The climatology (1950–1999) is depicted by the *black contours*

4.2 Methodology and results

In a first step, links between Sahelian rainfall and the inter-hemispheric SST gradient at global scale were highlighted for the CMIP3 models using a simple linear correlation approach. An index characterizing the SST inter-hemispheric mode (SSTIH) was then defined as the difference between normalized northern hemisphere SST (i.e. 10°N–70°N) and southern hemisphere ones (i.e. 60°S–10°N). The Sahelian rainfall index (SRI) was computed over the same area described previously (continental rainfall over

10°N–20°N, 16°W–45°E). This was carried out for the summer monsoon period (JAS), for both simulations and observations (CRUTS2.0 for rainfall, ERSSTv2 SST data set), the data being first low pass-filtered with an 8 year cut-off. Correlation coefficients between SRI and SSTIH were then plotted (Fig. 11a) as a function of the model skill in capturing the Sahelian rainfall low frequency variability (correlation between observed and simulated SRI). The coloured dots depict correlations for the period 1950–1999 while the dashed line tip shows the values computed over the twenty-first century (2001–2099). High positive

Fig. 10 **a** Mean seasonal (JAS) rainfall changes (*shading*) as simulated by the IPCC multi model ensemble mean (2070–2099 SRESA1B emission scenario minus 1950–1999 historical experiment). **b** Multi-model spread, defined as one standard deviation of the multi-model mean changes with respect to the ensemble mean. The *black contours* depict the ensemble mean climatology ones. The *dotted area* denotes significant changes at the 5% significance level as estimated by a student *t* test

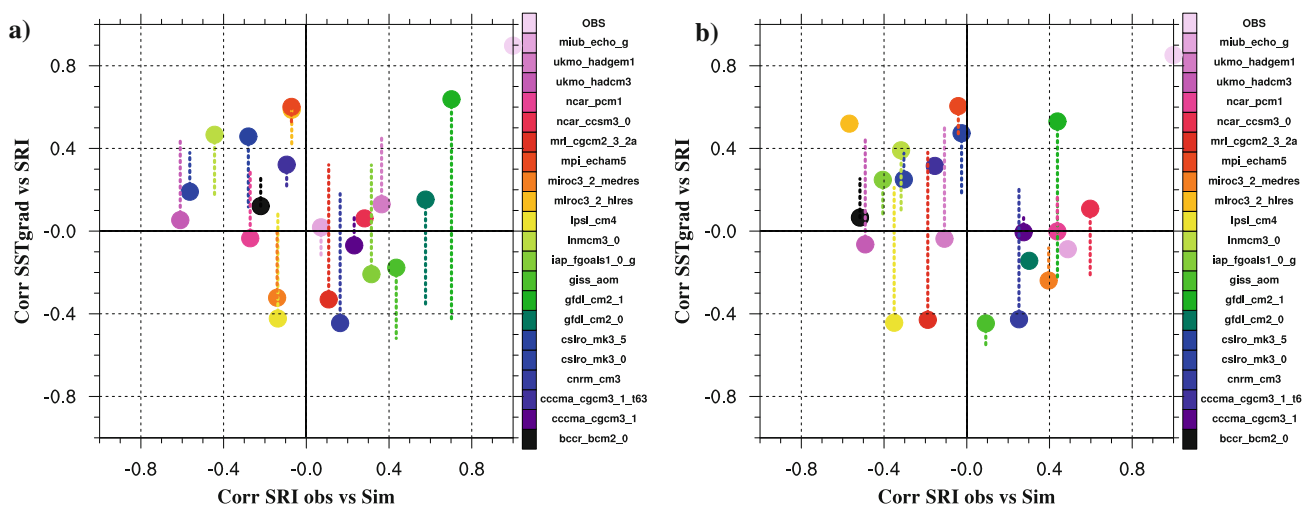
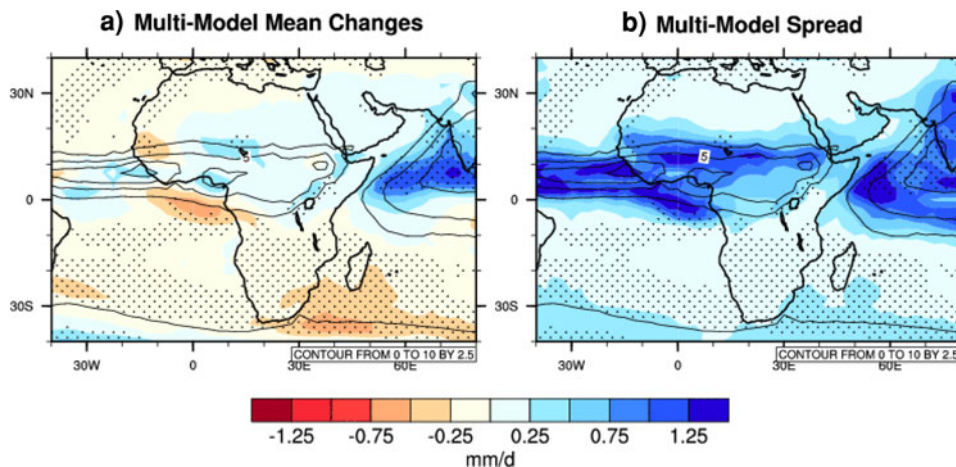


Fig. 11 **a** Scatter diagram of the correlation coefficients between the SRI and the inter-hemispheric SST gradient index (y axis) as a function of the correlations between modelled and observed SRI (x axis). The inter-hemispheric SST gradient index is defined as the difference between normalized northern hemisphere SST i.e. 10°N–70°N and southern hemisphere ones i.e. 60°S–10°N. Each

colored dot corresponds to a specific model; the correlations are computed over the 1950–1999 period (20c3m experiment). The *vertical bar* end denotes the correlation values computed over the twenty-first century (SRESA1B scenario, 2001–2099 period). All the data have been previously low-pass filtered with an 8 year cut-off. **b** The data have been previously linearly detrended

correlations are shown between observed SRI and SSTIH (about 0.92), and the observed SRI is obviously perfectly correlated (1) with itself (light pink dot). The model dots closed to this reference point denote both a good representation of Sahelian rainfall variability and a consistent link between Sahelian precipitation and the inter-hemispheric SST pattern over the second half of the twentieth century.

Only one model (gfdl_cm2_1) simulates both a consistent time-phased drying of the Sahel and consistent correlations with the global inter-hemispheric SST mode over the period 1950–1999. Good correlations between observed and simulated SRI are shown too for both gfdl_cm2_1 and giss_aom models ($r > 0.4$), but the “expected” correlation between SRI and SSTIH is

relatively weak for these models. Note that all these results remain consistent over this period applying different filter cut-off (above eight year, not shown). Note also that if the time period is extended to 1930–1999, and if a 10 year low-pass filter is applied, the correlation values for both versions of the GFDL model are similar (but the most skilful model remains gfdl_cm2_1, not shown). Nevertheless, given the retained criteria, although the gfdl_cm2_1 model can be argued to be a “hit model” over the recent past, the simulated links between SRI and SSTIH over the twenty-first century mismatch the “recent climate” assumptions. Indeed, the sign of the correlation changes for this model (about -0.42) for the future. In other words, although a significant decreasing rainfall trend is still simulated by the gfdl_cm2_1 model over the Sahel for the

twenty-first century (not shown), the northern hemisphere oceans warm up slightly faster than the southern oceans over this period. This suggests that the retained mechanism linking the global meridional SST gradient and the ITCZ location does not work for this model in SRESA1B (when the trend is retained), and illustrates the difficulty of defining a consistent metric for simulated rainfall changes over the sub-Saharan region. Namely, a model showing both time-phased Sahelian drought and consistent SST link for present climate does not necessary mean that it will follow the same behaviour for the future. Other elements will be given in the discussion section.

Using the same methodology, we focus on the co-variability between simulated sub-Saharan rainfall and mean tropospheric temperature for the CMIP3 models. Correlations coefficients between the SRI and a Tropospheric Temperature Index [hereafter TTI, defined as the tropical (30°S–30°N) temperature weighted average between 300 hPa and 700 hPa] are now plotted as a function of correlations between modeled and observed SRI (Fig. 12a). As there are no consistent tropospheric (3D) temperature observed satellite data set over the whole 1950–1999 time period we selected not to plot the observations. The NCEP/NCAR reanalysis are available, but as previously argued, there are many limitations for these data before 1970 over the tropics (Kinter et al. 2004). Nevertheless, even if not displayed on Fig. 12a, it can be noted that the correlation between NCEP TTI and CRUTS2.0 SRI is approximately -0.39 . Negative correlations between TTI and SRI are thus expected, as a warming of the free troposphere over the

tropics should lead to a reduction of deep convection over Africa.

Considering the 3 CMIP3 “hit” models that fairly well reproduced the time-phased Sahelian rainfall variability at decadal time scale over the second half of the twentieth century (giss_aom, gfdl_cm2_0 and gfdl_cm2_1), only giss_aom and gfdl_cm2_1 depict high negative correlations (-0.62 and -0.46 , respectively) between SRI and TTI. For future climate (twenty-first century), the negative correlation values significantly increase for both version of the GFDL model, whereas they become positive for giss_aom. This means that the tropospheric temperature increase over the tropics is not expected to play a role upon Sahelian rainfall within giss_aom, whereas, to some extent, a significant linear link between the increasing TT and Sahelian rainfall can be shown for both versions of the GFDL model over the twenty-first century. These results are consistent with those highlighted in the study of Held et al. (2005). Indeed, sensitivity experiments achieved with the atmospheric component of this model (AM2.1) show that the model is very sensitive to a uniform warming of global SST conditions. The atmospheric model was able to reproduce the Sahelian drought when forced only by a uniform global ocean warming of 2 K. Obviously, more sensitivity experiments should be performed with this model to highlight if the African rainfall response is clearly due to tropical or global SST causes. Nevertheless, the TT warming could be suggested to be a consistent mechanism to explain why these models simulate the observed drought, and moreover, why they simulate enhanced dry

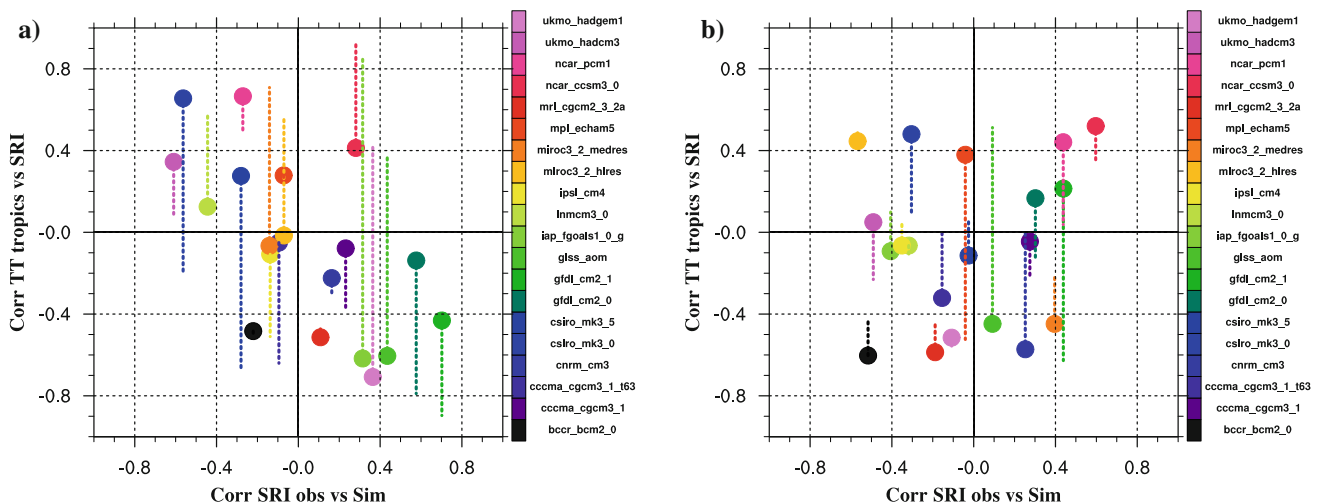


Fig. 12 a Scatter diagram of the correlation coefficients between the SRI and the tropospheric temperature index (y axis) as a function of the correlations between modelled and observed SRI (x axis). The tropospheric temperature index is defined as the weighted tropical (30°S–30°N) temperature average between 300 and 700 hPa. Each colored dot corresponds to a specific model; the correlations are

computed over the 1950–1999 period (20c3m experiment). The vertical bar end denotes the correlation values computed over the twenty-first century (SRESA1B scenario, 2001–2099 period). All the data have been previously low-pass filtered with an 8 year cut-off. b The data have been previously linearly detrended

conditions over the Sahel at the end of the twenty-first century without exhibiting any links with the SST meridional gradient at global scale for this period.

The CMIP3 coupled models in which the atmospheric model component is ARPEGE (cnrm_cm3 and bccr_bcm2_0) do not fit the two mechanisms highlighted previously using a “SST forced” approach. They both simulate a rainfall increase over the Guinea coast and a decrease over East Africa/Saudi Arabia at the end of the twenty-first century (zonal dipolar anomalies), this pattern being similar to the main decadal to multi-decadal variability modes (not shown). In these coupled models, the Atlantic tropical ocean warms up, resulting in increased ascending (descending) motions over the western coast (East/North–East) of Africa (not shown). It seems that they behave similarly to the ATL sensitivity experiment (Sect. 3.3), with slight regional differences as the simulated rainfall climatology extends northward over east Africa for these coupled models. These models fail to reproduce the Atlantic cold tongue (leading to warmer SST over the Gulf of Guinea), and consequently, this bias could be amplified in the future scenario simulations.

As an 8 year low pass filter has been applied to the time series in this analysis, decadal to multi-decadal variability is considered. In order to determine if the “high” correlations values for the “hit models” are associated with either the multi-decadal trend or with decadal oscillations, the same analysis has been performed removing the trend first (Fig. 11b, 12b). The correlations between observed and simulated SRI values decrease ($r = 0.4$) for the

gfdl_cm2_1 model for the present period when removing a linear trend (Fig. 11b). However, the relationship between the simulated SST and the SRI remains relatively high ($r = 0.5$), and the same behaviour can be highlighted for the observations. This indicates that the inter-hemispheric SST gradient can be related to the observed Sahelian rainfall variability at both decadal and multi-decadal time scales over the period 1950–1999. For the future, the correlation values between the SRI and the SST index are mainly associated with the trend. Concerning the SRI/TT relationship, high negative correlations are mainly related to the trend for both recent and future climate (Fig. 12b) for the gfdl model.

To further verify if the relationships between the SRI and the two proposed mechanisms are unchanged between the twentieth and the twenty-first century, a simple bi-variate regression model is used. To rebuild the SRI, the retained predictors are the TTI and SSTHI. The regression is trained from 1901 to 1999 for the 20c3m simulations. All data are low pass filtered with an eight year cut-off. The same method is then employed but all data are first linearly detrended. Correlations between predicted and simulated SRI for both 20c3m and SRESA1B experiments are then displayed on Fig. 13a (raw) and b (no trend). When accounting for the trend (Fig. 13a), the vast majority of models (excepting giss_aom, iap_fgoals and incm_3) show consistent SRI/TT/SST relationships between the twentieth and the twenty-first century. For the hit model (gfdl_cm2_1), the correlation increases in SRESA1B with respect to 20c3m. However, when removing the centennial

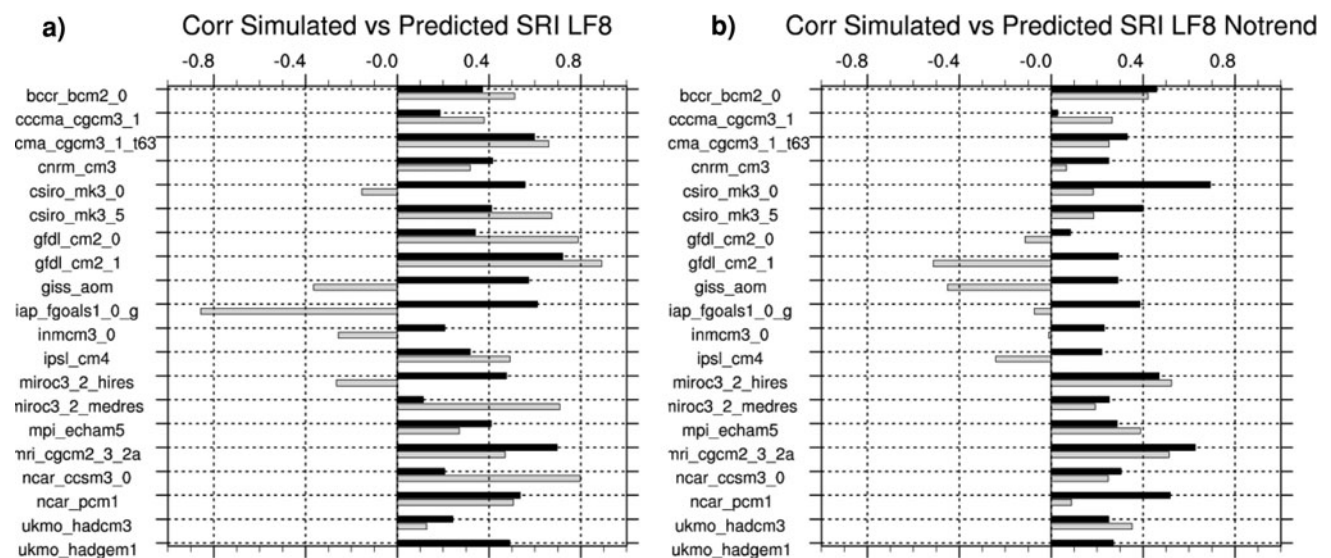


Fig. 13 Correlations between simulated and linearly predicted SRI in the 20c3m integrations (black 1901–1999) and the SRESA1B scenario simulations (gray 2001–2099). **a** The regression coefficients come from JAS SRI, the tropospheric temperature index and the

global SST gradient index, all the data have been previously low-pass filtered with an 8 year cut-off. **b** Idem, but all data have been previously detrended

trend, this relationship does not remain consistent for *gfdl_cm2_1* for the twenty-first century. In addition, the high correlation values between simulated and predicted SRI (Fig. 13a) are mainly related to the TT warming (and tropical Indo-Pacific SST) rather than the global SST gradient for *gfdl_cm2_1*. Supplementary details are given in the discussion section.

In conclusion, very few CMIP3 coupled models are able to both reproduce the observed drying over the Sahel and to fit the two plausible mechanisms of tropospheric temperature and SST meridional gradient highlighted in this work. However, the *gfdl_cm2_1* model simulates both features over the second half of the twentieth century. This model predicts enhanced Sahel dry conditions for the twenty-first century, partly related to a warming of global oceanic and tropical tropospheric temperatures. Even if this model simulates realistic features of Sahelian rainfall variability over the recent past, it may be oversensitive to the SST/TT rising for the future. However, our results converge with those highlighted in Held et al. (2005), namely that the prediction of twenty-first century drying over sub-Saharan Africa could be considered as a plausible but not certain scenario.

4.3 Limitations and discussion

There are numerous limitations to this study that must be mentioned.

Obviously, correlation does not mean causality, and additional sensitivity experiments should be carried out to characterize the simulated Sahelian rainfall sensitivity to both SST/TT anomalies. However, this has been partly done for the ARPEGE model in this study and for the GFDL model in the work of Held et al. (2005).

Ranking the CMIP3 coupled models according to the correlation coefficients between observed and simulated SRI could have a limited meaning. Indeed, one would expect good correlations between SRI in a coupled simulation and the observation only if the forced (natural and anthropogenic) component of the SST signal is dominant. However, the internal SST variability in these coupled simulations could play a significant role. For example, the Atlantic Multidecadal Oscillation (AMO), often referred to as an internal mode of climate variability, is associated to the Sahelian drought in the work of Zhang and Delworth (2006). The importance of forced versus internal variability of the SST signal in the CMIP3 coupled simulations has not been quantified in this study but should be carried out comparing the preindustrial experiments to historical simulations (20c3m). Here, we have made the underlying assumption that the model could simulate the observed decadal to multi-decadal rainfall variability over the Sahel (and consistent SST variability) under realistic external forcing (anthropogenic and natural) over the twentieth

century. Note also that only one realization is considered for each model in this work.

The links between Sahelian rainfall and SST have only been highlighted here at global scale (global meridional SST gradient), and not at regional scale (link between each oceanic basin and sub-saharan rainfall). An extended overview for the recent period is given in the study of Lau et al. (2006) for the recent period, and for control, historical present climate and future IPCC scenario simulations in the recent study of Biasutti et al. (2008).

Based on a bi-variate regression model predicting rainfall variations from changes in Indo-Pacific SST and Atlantic SST meridional gradient for the control (pre-industrial) CMIP3 runs, the authors show that the inter-annual to multi-decadal rainfall variability over the Sahel can be skilfully reproduced for most of the historical experiments (20c3m) runs. However, this statistical model then fails in reproducing the twenty-first centennial trend for a vast majority of models.

The intention is that few consensuses can be proposed. Namely, that a model can both reproduce a time-phased drought over the Sahel and a consistent link with the SST over the twentieth century does not mean it will behave the same for the future when accounting for the trend in the global warming signal. This shows the difficulty (even the impossibility) of using a metric based on recent SST/SRI relationships to confidently predict rainfall changes over the Sahel for the future.

Returning to Table 1, other surface and atmospheric mechanisms could play an active role in driving Sahelian rainfall changes for the future. For example, a deepening of the heat low (expected as the Sahara warms up in all the future climate change simulations), could lead to a moistening of the Sahel (Haarsma et al. 2005). Moreover, as the atmosphere is expected to warm up, an intensification of the hydrological cycle over the main monsoon areas could be conceivable, since a warmer atmosphere is expected to hold more water. All these plausible mechanisms could counteract regionally the expected drying impact of warmer tropospheric temperatures over the tropics, leading to strong uncertainties in predicting sub-Saharan rainfall change over the twenty-first century.

5 Conclusions

The ability of the ARPEGE AGCM to reproduce the twentieth century Sahelian drought has been assessed. This task has been achieved using both AMIP-like ensemble simulations forced by prescribed SST time evolution and sensitivity experiments. Analysis of ensemble simulations confirmed that the basic structure of the Sahel drought can be simulated when the model only uses the observed SST

as lower boundary conditions. However, the simulated precipitation decrease is mainly located over central and eastern Africa and underestimated. Furthermore, atmospheric internal variability has been shown to contribute strongly to precipitation variability over the Sahel at decadal to multi-decadal time scale. Based on the ARPEGE ensemble simulation analysis, the simulated drought is associated with a southward shift of the rainbelt over the Sahel and linked with an inter-hemispheric SST mode. Analysis of idealized experiments further demonstrates the importance of the tropical Pacific basin in driving the simulated Sahelian rainfall anomalies. The warming of the Pacific partly leads to a homogeneous increase of the tropospheric temperature (TT) over the tropics. This leads to enhanced dry advection from the Sahara to the Sahel in agreement with the so-called “upped-ante” mechanism. Nevertheless, the Pacific/Sahel teleconnection mechanism highlighted here should be considered with the greatest caution, as it is likely to be strongly model-dependent.

Historical and scenario experiments from the CMIP3 multi-model data base have been examined to study simulated rainfall changes over the Sahel at the end of the twenty-first century. The different model projections for Sahel rainfall changes in response to global warming remain highly uncertain. Relying on our model results and the highlighted consensus with previous published works, the accuracy of the CMIP3 models in both reproducing the observed Sahelian drought and the two previously highlighted mechanisms over the twentieth century and for the future has been examined.

From a simple analysis, we conclude that only the GFDL model simulates both a consistent Sahel drying and a consistent relationship between Sahelian rainfall, the interhemispheric SST gradient and tropical tropospheric temperatures for the 1950–1999 period. This model predicts enhanced dry conditions over sub-Saharan Africa at the end of the twenty-first century. However, even if this model skilfully simulates the relationship between the global SST gradient and Sahelian rainfall for the recent climate, this relationship is not consistent for the future. As a consequence, it shows the difficulty to build a consistent “model” metric based on observed SST/SRI relationships to get a trustworthy prediction of the future climate over the Sahelian region.

It appears that future rainfall change over the Sahel cannot be controlled by only SST/TT mechanisms. Indeed, the influence of surface conditions (vegetation, land use, soil moisture) has not been considered in this study. Surface conditions might also play a crucial role in driving future rainfall changes over the Sahel. The complexity of studying future rainfall changes over sub-Saharan Africa mainly consists of the different competing/complementary mechanisms that can play a role under enhanced GHG

conditions (Table 1) and their representation in the current AOGCMs. The representation of these mechanisms by climate models needs to be investigated using a multi-model sensitivity experiment approach. This should be highlighted within the AMMA international project framework, in which numerous soil moisture/SST sensitivity experiments will be produced for several models. Moreover, many observational campaigns have been carried out during AMMA. Comparing the model sensitivities to crucial mechanisms which can occur under a warmer climate and comparing them to consistent observations will increase our knowledge of the African monsoon system and will allow improving the GCM parameterization for the next IPCC assessment.

Acknowledgments This work was supported by the African Monsoon Multidisciplinary Analysis (AMMA) project and by the European Community via the sixth framework ENSEMBLE project under Contract GOCE-CT-2003-505539. The authors are grateful to all IPCC4 participants and to PCMDI for the build up of the database.

References

- Bader J, Latif M (2003) The impact of decadal-scale Indian Ocean sea surface temperature anomalies on Sahelian rainfall and the north Atlantic oscillation. *Geophys Res Lett* 30(22):2169. doi:[10.1029/2003GL018426](https://doi.org/10.1029/2003GL018426)
- Biasutti M, Giannini A (2006) Robust Sahel drying in response to late twentieth century forcings. *Geophys Res Lett* 33. doi:[10.1029/2006GLO26067](https://doi.org/10.1029/2006GLO26067)
- Biasutti M, Held IM, Giannini A, Sobel AH (2008) SST forcings and Sahel rainfall variability of the twentieth and twenty-first centuries. *J Clim* (submitted). http://www.gfdl.noaa.gov/~ih/papers/biasutti_et al.pdf
- Bougeault P (1985) A simple parametrization of the large scale effects of deep cumulus convection. *Mon Weather Rev* 113: 2108–2121. doi:[10.1175/1520-0493\(1985\)113<2108:ASPOTL>2.0.CO;2](https://doi.org/10.1175/1520-0493(1985)113<2108:ASPOTL>2.0.CO;2)
- Camberlin P, Janicot S, Pocard I (2001) Seasonality and atmospheric dynamics of the teleconnections between Africa and tropical Ocean surface temperature: Atlantic versus ENSO. *Int J Clim* 21:973–1005. doi:[10.1002/joc.673](https://doi.org/10.1002/joc.673)
- Caminade C, Terray L (2006) Influence of increased greenhouse gases and sulphate aerosols concentration upon diurnal temperature range over Africa at the end of the twentieth century. *Geophys Res Lett* 33:L15703. doi:[10.1029/2006GL026381](https://doi.org/10.1029/2006GL026381)
- Charney JG, Quirk WJ, Show SH, Kornfield J (1977) A comparative study of the effects of albedo change on drought in semiarid regions. *J Atmos Sci* 34:1366–1385. doi:[10.1175/1520-0469\(1977\)034<1366:ACSOTE>2.0.CO;2](https://doi.org/10.1175/1520-0469(1977)034<1366:ACSOTE>2.0.CO;2)
- Chiang J, Sobel A (2002) Tropical tropospheric temperature variations caused by ENSO and their influence on the remote tropical climate. *J Clim* 15:2616–2631. doi:[10.1175/1520-0442\(2002\)015<2616:TTVCB>2.0.CO;2](https://doi.org/10.1175/1520-0442(2002)015<2616:TTVCB>2.0.CO;2)
- Chou C, Neelin JD (2004) Mechanisms of global warming impacts on regional tropical precipitation. *J Clim* 17(13):2688–2701. doi:[10.1175/1520-0442\(2004\)017<2688:MOGWIO>2.0.CO;2](https://doi.org/10.1175/1520-0442(2004)017<2688:MOGWIO>2.0.CO;2)
- Déqué M (1999) Documentation ARPEGE-CLIMAT. Tech report Centre National de Recherche Météorologiques, Météo-France, Toulouse, France

- Déqué M, Drevet C, Braun A, Cariolle D (1994) The climate version of the ARPEGE-IFS: a contribution of the French community climate modeling. *Clim Dyn* 10:249–266. doi:[10.1007/BF00208992](https://doi.org/10.1007/BF00208992)
- Douville H (2003) Assessing the influence of soil moisture on seasonal climate variability with AGCMs. *J Clim* 14:1044–1066
- Douville H, Salas Méliá D, Tytéca S (2006) On the tropical origin of uncertainties in the global land precipitation response to global warming. *Clim Dyn* 26:367–385. doi:[10.1007/s00382-005-0088-2](https://doi.org/10.1007/s00382-005-0088-2)
- Folland CK, Palmer TN, Parker DE (1986) Sahel rainfall and worldwide sea surface temperature 1901–1985. *Nature* 320:602–607. doi:[10.1038/320602a0](https://doi.org/10.1038/320602a0)
- Fontaine B, Janicot S (1992) Wind field coherence and its variations over West Africa. *J Clim* 5:512–524. doi:[10.1175/1520-0442\(1992\)005<0512:WFAIV>2.0.CO;2](https://doi.org/10.1175/1520-0442(1992)005<0512:WFAIV>2.0.CO;2)
- Giannini A, Saravanan R, Chang P (2003) Oceanic forcing of Sahel rainfall on interannual to interdecadal time scales. *Science* 302:1027–1030. doi:[10.1126/science.1089357](https://doi.org/10.1126/science.1089357)
- Grist JP, Nicholson SE (2001) A study of dynamics factor influencing the rainfall variability in the West African Sahel. *J Clim* 14:1337–1359. doi:[10.1175/1520-0442\(2001\)014<1337:ASOTDF>2.0.CO;2](https://doi.org/10.1175/1520-0442(2001)014<1337:ASOTDF>2.0.CO;2)
- Haarsma RJ, Selten FM, Weber SL, Kliphuis M (2005) Sahel rainfall and response to greenhouse warming. *Geophys Res Lett* 32. doi:[10.1029/2005GLO23232](https://doi.org/10.1029/2005GLO23232)
- Hastenrath S (1990) Decadal-scale changes of the circulation in the tropical Atlantic sector associated with Sahel drought. *Int J Clim* 10:459–472. doi:[10.1002/joc.3370100504](https://doi.org/10.1002/joc.3370100504)
- Held IM, Delworth TL, Lu J, Findell KL, Knutson TR (2005) Simulation of Sahel drought in the twentieth and twenty-first centuries. *Proc Nat Acad Sci USA* 102:17891–17896. doi:[10.1073/pnas.0509057102](https://doi.org/10.1073/pnas.0509057102)
- Herceg D, Sobel A, Sun L (2007) Regional modelling of decadal rainfall variability over the Sahel. *Clim Dyn* 29:88–99. doi:[10.1007/s00382-006-0218-5](https://doi.org/10.1007/s00382-006-0218-5)
- Hoerling MP, Hurrell JW, Eischeid J (2006) Detection and attribution of twentieth century northern and southern Africa monsoon change. *J Clim* 19:3989–4008. doi:[10.1175/JCLI3842.1](https://doi.org/10.1175/JCLI3842.1)
- Janicot S, Trzaska S, Pocard I (2001) Summer Sahel-ENSO teleconnection and decadal time scale SST variations. *Clim Dyn* 18:303–320. doi:[10.1007/s003820100172](https://doi.org/10.1007/s003820100172)
- Joly M, Voltaire A, Douville H, Terray P, Royer JF (2007) African monsoon teleconnections with tropical SSTs: validation and evolution in a set of IPCC4 simulations. *Clim Dyn*. doi:[10.1007/s00382-006-0215-8](https://doi.org/10.1007/s00382-006-0215-8)
- Kinter J, Fennessy M, Krishnamurthy V, Marx L (2004) An evaluation of the apparent interdecadal shift in the tropical divergent circulation in the NCEP–NCAR reanalysis. *J Clim* 17:349–361. doi:[10.1175/1520-0442\(2004\)017<0349:AEOTAI>2.0.CO;2](https://doi.org/10.1175/1520-0442(2004)017<0349:AEOTAI>2.0.CO;2)
- Lamb PJ (1978) Large scale tropical surface circulation patterns associated with sub-Saharan weather anomalies. *Tellus* 30:240–251
- Lau KM, Shen SSP, Kim KM, Wang (2006) A multimodel study of the twentieth century simulations of Sahel drought from the 1970s to 1990s. *J Geophys Res* 11:DO7111. doi:[10.1029/2005JD006821](https://doi.org/10.1029/2005JD006821)
- Louis JF, Tiedtke M, Geleyn JF (1981) A short history of the operational PBL-parameterization at ECMWF. In: ECMWF workshop planetary boundary layer parameterization, 25–27 Nov 1981, ECMWF, Reading, UK, pp 59–80
- Lu J, Delworth T (2005) Oceanic forcing of the late twentieth century Sahel drought. *Geophys Res Lett* 32. doi:[10.1029/2005GLO23316](https://doi.org/10.1029/2005GLO23316)
- Mahfouf JF, Manzi AO, Noilhan J, Giordani H, Déqué M (1995) The land surface scheme ISBA within the Météo France climate model ARPEGE. Part I: implementation and preliminary results. *J Clim* 8:2039–2057. doi:[10.1175/1520-0442\(1995\)008<2039:TLSSIW>2.0.CO;2](https://doi.org/10.1175/1520-0442(1995)008<2039:TLSSIW>2.0.CO;2)
- Mehta VM, Suarez MJ, Manganello JV, Delworth TL (2000) Oceanic influence on the north Atlantic oscillation and associated northern Hemisphere climate variations: 1959–1993. *Geophys Res Lett* 27(1):121–124. doi:[10.1029/1999GL002381](https://doi.org/10.1029/1999GL002381)
- Mitchell T, Jones P (2005) An improved method of constructing a database of monthly climate observations and associated high resolution grids. *Int J Clim* 25:693–712. doi:[10.1002/joc.1181](https://doi.org/10.1002/joc.1181)
- Morcrette JJ (1990) Impact of changes to radiation transfer parameterizations plus cloud optical properties in the ECMWF model. *Mon Weather Rev* 118:847–873. doi:[10.1175/1520-0493\(1990\)118<0847:IOCTTR>2.0.CO;2](https://doi.org/10.1175/1520-0493(1990)118<0847:IOCTTR>2.0.CO;2)
- Neelin JD, Chou C, Su H (2003) Tropical drought regions in global warming and El Niño teleconnections. *Geophys Res Lett* 30(24):2275. doi:[10.1029/2003GL018625](https://doi.org/10.1029/2003GL018625)
- Noilhan J, Planton S (1989) A simple parameterization of land surface processes for meteorological models. *Mon Weather Rev* 117:536–549. doi:[10.1175/1520-0493\(1989\)117<0536:ASPOLS>2.0.CO;2](https://doi.org/10.1175/1520-0493(1989)117<0536:ASPOLS>2.0.CO;2)
- Palmer TN (1986) Influence of the Atlantic, Pacific and Indian oceans on Sahel rainfall. *Nature* 322:251–253. doi:[10.1038/322251a0](https://doi.org/10.1038/322251a0)
- Pocard I, Janicot S, Camberlin P (2000) Comparison of rainfall structures between NCEP and NCAR reanalysis and observed data over Africa. *Clim Dyn* 16:897–915. doi:[10.1007/s003820000087](https://doi.org/10.1007/s003820000087)
- Ricard JL, Royer JF (1993) A statistical cloud scheme for use in AGCM. *Ann Geophys* 11:1095–1115
- Rowell DP (2001) Teleconnections between the tropical Pacific and the Sahel. *Q J R Meteorol Soc* 127:1683–1706. doi:[10.1002/qj.49712757512](https://doi.org/10.1002/qj.49712757512)
- Rowell DP, Zwiers FW (1999) The global distribution of sources of atmospheric decadal variability and mechanisms over the tropical Pacific and southern North America. *Clim Dyn* 15:751–772. doi:[10.1007/s003820050314](https://doi.org/10.1007/s003820050314)
- Smith T, Reynolds R (2004) Improved extended reconstruction of SST (1854–1997). *J Clim* 17:2466–2477. doi:[10.1175/1520-0442\(2004\)017<2466:IEROS>2.0.CO;2](https://doi.org/10.1175/1520-0442(2004)017<2466:IEROS>2.0.CO;2)
- Su H, Neelin J, Meyerson J (2005) Mechanism for lagged atmospheric response to ENSO SST forcing. *J Clim* 18:4195–4215. doi:[10.1175/JCLI3514.1](https://doi.org/10.1175/JCLI3514.1)
- Yulaeva E, Wallace J (1994) The signature of ENSO in global temperature and precipitation fields derived from the microwave sounding unit. *J Clim* 7:1719–1736. doi:[10.1175/1520-0442\(1994\)007<1719:TSEOIG>2.0.CO;2](https://doi.org/10.1175/1520-0442(1994)007<1719:TSEOIG>2.0.CO;2)
- Zhang R, Delworth TL (2006) Impact of Atlantic multidecadal oscillations on India/Sahel rainfall and Atlantic hurricanes. *Geophys Res Lett* 33:L17712. doi:[10.1029/2006GL026267](https://doi.org/10.1029/2006GL026267)
- Zwiers F (1996) Interannual variability and predictability in an ensemble of AMIP climate simulations conducted with the CCC GCM2. *Clim Dyn* 12:825–848. doi:[10.1007/s003820050146](https://doi.org/10.1007/s003820050146)